iScience

CellPress

Article

Commensal Gut Bacteria Buffer the Impact of Host Genetic Variants on *Drosophila* Developmental Traits under Nutritional Stress

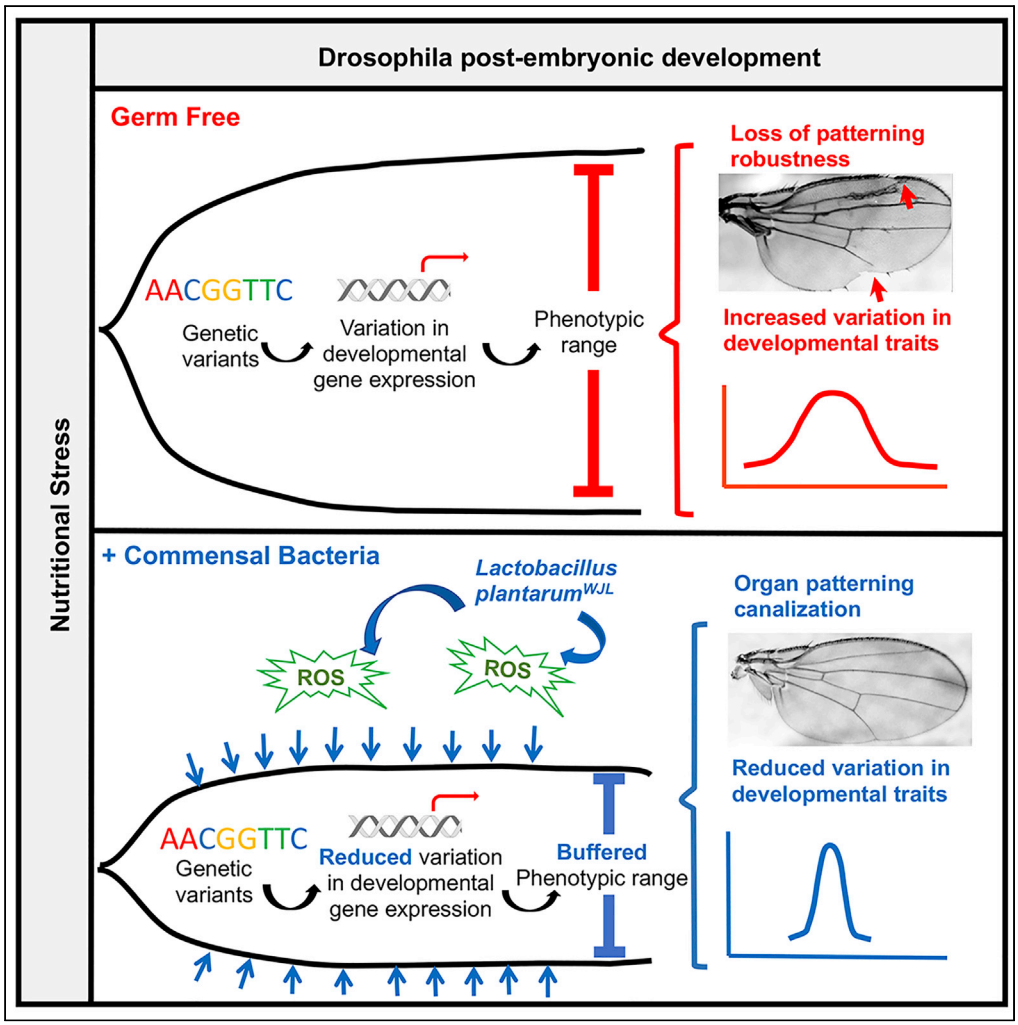

Dali Ma, Maroun Bou-Sleiman, Pauline Joncour, ..., Gilles Storelli, Bart Deplancke, François Leulier

bart.deplancke@epfl.ch (B.D.)
francois.leulier@ens-lyon.fr (F.L.)

HIGHLIGHTS

Upon nutritional stress, fly commensals buffer the effects of cryptic genetic variants

Fly gut commensals buffer transcriptional variation in developmental genes

Fly commensals buffer phenotypic heterogeneity and mediate developmental canalization

Compromising ROS activities impair microbial buffering capacity

Ma et al., iScience *19*, 436–447
September 27, 2019
https://doi.org/10.1016/j.isci.2019.07.048

iScience

CellPress

Article

Commensal Gut Bacteria Buffer the Impact of Host Genetic Variants on *Drosophila* Developmental Traits under Nutritional Stress

Dali Ma,[1] Maroun Bou-Sleiman,[2,3] Pauline Joncour,[1] Claire-Emmanuelle Indelicato,[1] Michael Frochaux,[2] Virginie Braman,[2] Maria Litovchenko,[2] Gilles Storelli,[1,4] Bart Deplancke,[2,5,*] and François Leulier[1,5,6,*]

SUMMARY

Eukaryotic genomes encode several buffering mechanisms that robustly maintain invariant phenotypic outcome despite fluctuating environmental conditions. Here we show that the *Drosophila* gut-associated commensals, represented by a single facultative symbiont, *Lactobacillus plantarum* (Lp^{WJL}), constitutes a so far unexpected buffer that masks the contribution of the host's cryptic genetic variation (CGV) to developmental traits while the host is under nutritional stress. During chronic under-nutrition, Lp^{WJL} consistently reduces variation in different host phenotypic traits and ensures robust organ patterning during development; Lp^{WJL} also decreases genotype-dependent expression variation, particularly for development-associated genes. We further provide evidence that Lp^{WJL} buffers via reactive oxygen species (ROS) signaling whose inhibition impairs microbiota-mediated phenotypic robustness. We thus identified a hitherto unappreciated contribution of the gut facultative symbionts to host fitness that, beyond supporting growth rates and maturation timing, confers developmental robustness and phenotypic homogeneity in times of nutritional stress.

INTRODUCTION

The concept of developmental robustness, or "canalization," was first introduced by Conrad Waddington to illustrate the organisms' capacity to maintain constant and invariant phenotypic outcome in the presence of fluctuating environmental conditions and certain genetic perturbations (Huang et al., 2014; Mackay et al., 2012; Waddington, 1959). To achieve canalization, intrinsic genetic buffering programs are set in place to repress the effects of cryptic genetic variants (CGV). If these buffering mechanisms are compromised or overwhelmed by physiological or environmental stress, the CGVs can be "unlocked" to increase phenotypic variation and/or produce novel phenotypes for natural selection to act upon (Flatt, 2005; Wagner, 2007). So far, all known buffering mechanisms are encoded by the eukaryotic genome. The classic examples include the chaperone protein Hsp90 and certain microRNAs (Posadas and Carthew, 2014; Rutherford et al., 2007). Yet, the vast majority of living organisms can be viewed as the sum of the host and its associated microbial symbionts, as a result of long-term, constant, and heritable symbiosis. Whether these microbial symbionts also contribute to host developmental robustness is still poorly understood.

Symbiosis is ancient, pervasive, and diverse and in some instances is recognized as a major driving force of evolution (Brucker and Bordenstein, 2013; Gilbert, 2014). Facultative nutritional mutualism is one of the most prevalent forms of symbiosis forged by a eukaryotic host and many of its gut commensal bacteria, known collectively as the "gut microbiota." Recent studies have established that the microbial partners contribute extensively to various aspects of host physiology, and perturbing the healthy balance of gut microbial communities often leads to undesirable developmental and fitness consequences for the host (Clemente et al., 2012; Sommer and Backhed, 2013). The nomenclature "facultative nutritional symbiosis" suggests that both partners are nonessential for each other's survival, yet neither may thrive especially under suboptimal nutritional contexts (Gilbert and Neufeld, 2014). The horizontally acquired gut commensals in *Drosophila* are a prototypical example of such facultative nutritional mutualists. Recent studies established that certain wild fly gut bacterial isolates can establish persistent colonization of the host's crop, a digestive organ that is unique to the adult fly but is absent in the developing larvae (Obadia et al., 2018; Pais et al., 2018), where the gut community members that comprise the microbial environment are in fact non-persistent; instead they transit rapidly through the larval gut after being ingested, are reseeded, and proliferate in the food substrate. This "farming mechanism" effectively perpetuates a mutualistic

[1]Institut de Génomique Fonctionnelle de Lyon (IGFL), Université de Lyon, Ecole Normale Supérieure de Lyon, Centre National de la Recherche Scientifique, Université Claude Bernard Lyon 1, Unité Mixte de Recherche 5242, 69364 Cedex 07, Lyon, France

[2]Laboratory of Systems Biology and Genetics, Institute of Bioengineering and Swiss Institute of Bioinformatics, School of Life Sciences Ecole Polytechnique Federale de Lausanne (EPFL), 1015, Lausanne, Switzerland

[3]Present address: Laboratory of Integrative Systems Physiology, Interschool Institute of Bioengineering, School of Life Sciences, Ecole Polytechnique Federale de Lausanne (EPFL), 1015 Lausanne, Switzerland

[4]Present address: Department of Human Genetics, University of Utah School of Medicine, UT 84112, Salt Lake City, USA

[5]Senior author

[6]Lead Contact

*Correspondence: bart.deplancke@epfl.ch (B.D.), francois.leulier@ens-lyon.fr (F.L.)

https://doi.org/10.1016/j.isci.2019.07.048

interaction with the juvenile host and confers growth advantage to the host in different nutritional context (Ma and Leulier, 2018; Storelli et al., 2018). Here for the sake of simplicity, we refer to these non-persistently commensal bacteria as "gut-associate symbionts" or "gut commensals." Previously, we and others demonstrated that, on a standard laboratory diet, the gut commensals are dispensable for normal growth and maturation of the *Drosophila* host. It is only when challenged by chronic under-nutrition, germ-free (GF) larvae experienced significant growth delay (Shin et al., 2011; Storelli et al., 2011). In this context, a single gut commensal strain, *Lactobacillus plantarum*^{WJL} (*Lp*^{WJL}) (Kim et al., 2013), can significantly accelerate the growth of the ex-germ free larvae as effectively as the entire gut-associated microbial communities (Storelli et al., 2011).

To discover host genetic variants associated to the growth benefits conferred by *Lp*^{WJL} during chronic under-nutrition, we first exploited the *Drosophila* Genetic Reference Panel (DGRP) (Huang et al., 2014; Mackay et al., 2012) by performing a genome-wide association study on the relative growth gain of *Lp*^{WJL}-associated compared with GF DGRP lines. During this process, we discovered that the gut-associated symbionts, represented by *Lp*^{WJL}, assert a previously unappreciated role that functionally resembles a broad genetic buffer. Specifically, when subjected to nutritional stress, *Lp*^{WJL} effectively masks the effects of the host's CGVs on developmental traits, thus conveying phenotypic homogeneity and robustness in organ patterning via reactive oxygen species (ROS) signaling. Our results qualify the fly gut community as part of the extended-host's developmental canalization program.

RESULTS

Mono-Association with Lp^{WJL} Reduces Size Variation of Drosophila Larvae during Chronic Under-nutrition in the DGRP Lines

Initially, to study the host's genetic contribution to *Lp*^{WJL}-mediated growth during under-nutrition, we measured the body lengths of both the GF and *Lp*^{WJL} mono-associated larvae from 53 DGRP lines 7 days after post-embryonic development (Figures 1A–1C; Table S1) and conducted genome-wide association studies (GWAS) based on the ranking of growth gain by comparing GF and *Lp*^{WJL}-associated animals (Figure 1A; Table S1, column "ratio"). The GWAS yielded nine candidate variants (Table S2, Figures S1A and S1B). Through RNA interference (RNAi), we assessed the contribution of each variant-associated gene to host growth with or without *Lp*^{WJL}. Surprisingly, we failed to capture any obvious "loss or gain of function" of the growth benefit conferred by *Lp*^{WJL}. Instead, we observed that the individual RNAi-mediated knock-down of gene expression led to large phenotypic variation in GF larvae, but such variation was reduced in *Lp*^{WJL}, resulting in growth gain in all tested genetic crosses (Figures S1C and S1D). In parallel, we computed the respective heritability estimates (H) for the GF and *Lp*^{WJL}-associated DGRP populations to be 17% versus 6% (Figures 1B and 1C). Since the H values are low, we further examined the empirical distribution of the H values in the GF and *Lp*^{WJL}-associated populations and found that the H values of the GF samples span a significantly greater range (Figure 1D). Next, we compared the relative variability of the GF and mono-associated larval length. Since the *Lp*^{WJL}-associated larvae are twice the size of the GF larvae, we opted to compare the dimensionless coefficient of variation (CV) of the two populations and found that the CV is greater in the GF population despite their overall smaller average size and standard deviation (Figure 1E). These three observations indicate that genetic variants induce more pronounced size variation in GF animals, and the gut-associated symbiont such as *Lp*^{WJL} unexpectedly restricts growth variation despite host genetic differences. To better illustrate the buffering effect, we plotted the average GF larval length values from each DGRP line or each RNAi cross against its corresponding *Lp*^{WJL}-associated siblings and derived the linear regression coefficients and found that both are close to zero (0.145 and 0.06, respectively; Figures 1F and S1E). If genetic background predominantly impacts growth, then this coefficient is expected to approach one. The near-zero coefficient, the greater size variation, and the wider distribution of H values in the GF population prompts us to postulate that *Lp*^{WJL} presence masks the contribution of genetic variation in the DGRP lines and steers the animals to attain similar sizes despite the differences in genotype.

Mono-Association with Lp^{WJL} Decreases Variability in Gene Expression of Developmentally Related Genes

Since *Lp*^{WJL} reduces host growth variation phenotypically, and phenotypic variation is often the manifestation of transcriptomic variation due to genetic differences (Lehner, 2013), we explored if *Lp*^{WJL} also decreases gene expression variation during larval development. To do so, we conducted BRB-seq (Alpern et al., 2019) on 36 mono-associated and 36 GF individual larvae from 3 DGRP lines and specifically compared transcriptional

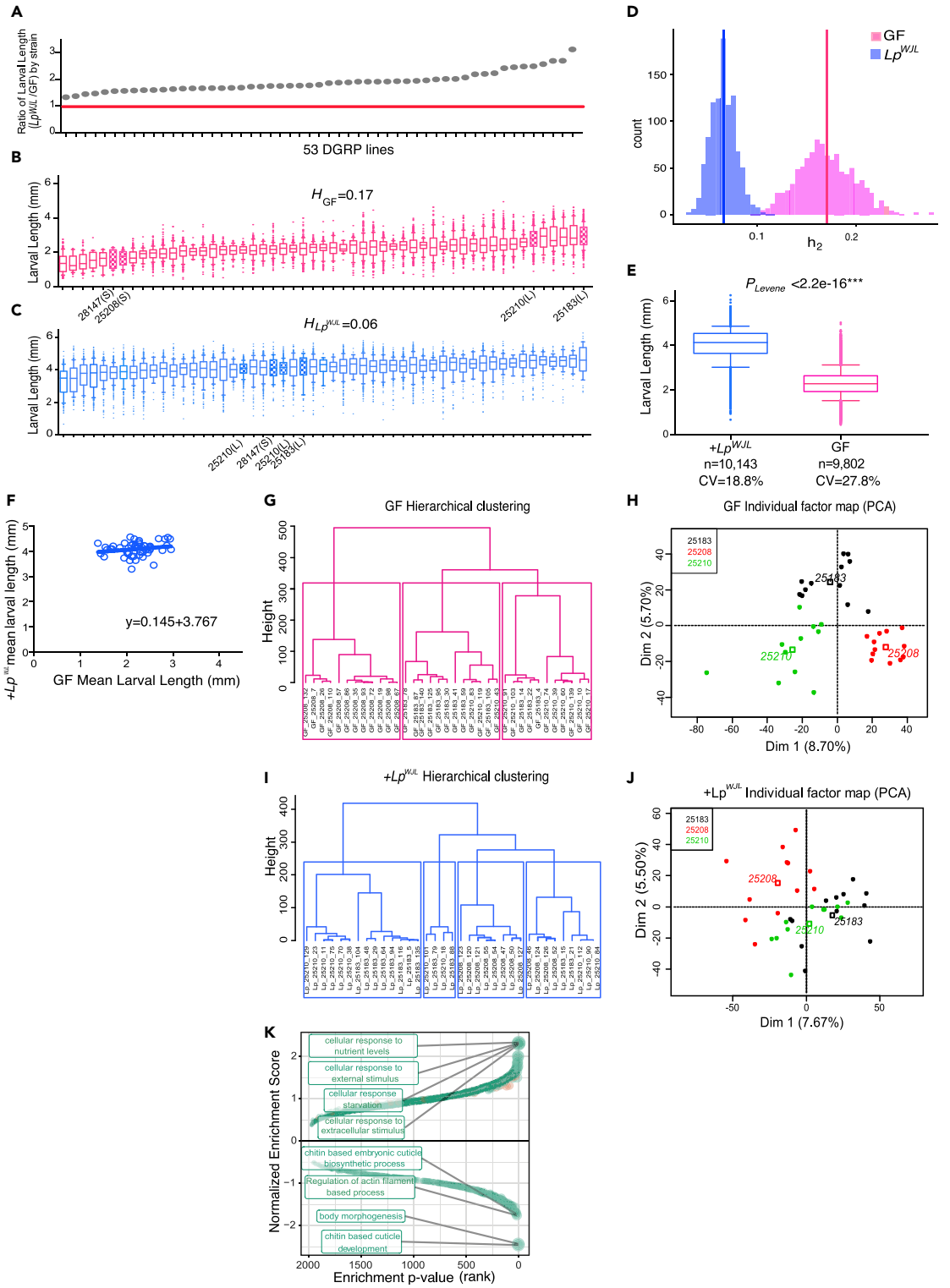

Figure 1. Mono-association with *Lp*^{WJL} Buffers Phenotypic and Transcriptomic Variation during Growth and Development in the DGRP Lines

(A) The ranking of larval growth gain of 53 DGRP lines was used for GWAS to uncover host variants associated with growth benefits conferred by *Lp*^{WJL}. Each gray dot represents the quotient of average mono-associated larval length (Figure 1C) divided by the average length of GF larval length (Figure 1B) from each DGRP line on Day 7 AEL (after egg lay). The red line marks the ratio of "1," indicating that all tested DGRP lines benefited from *Lp*^{WJL} presence.

Figure 1. *Continued*

(B and C) The average larval length on Day 7 AEL for each of the 53 DGRP lines. (Data are represented as mean and 10–90 percentile. Unless specified, all box plots in this manuscript present the same parameters.) Each line in the box represents the average length from pooled biological replicates containing all viable larvae from all experimental repeats. From each strain, there are between 10 and 40 viable larvae in each replicate, 3 biological replicates for each experiment, and 2 to 3 repeats of the experiments. (B): germ-free (GF, pink), (C): mono-associated (+Lp^{WJL}, blue). Note the heritability estimate (H) in the GF population is higher than in the mono-associated population (17% versus. 6%). The filled boxes denote the "small (S)" and "large (L)" DGRP lines that were selected for setting up the F_2 crosses (see Figure S3A for crossing schemes).

(D) The estimation of empirical distribution of heritability indices in GF and Lp^{WJL} mono-associated larvae ($p < 2.2 \times 10^{-16}$, Kolmogorov-Simirnov test). The vertical lines are reported H values.

(E) Box and whiskers plots showing average larval length derived from pooled GF (pink) or Lp^{WJL} (blue) mono-associated DGRP lines. The coefficient of variation in the GF population (27.82%) is greater than that of the mono-association population (18.74%). Error bars indicate 10th to 90th percentile. Levene's test is used to evaluate homocedasticity and Mann-Whitney test for difference in the median (***$p < 0.0001$).

(F) Scatterplot to illustrate that Lp^{WJL} buffers size variation in ex-GF larvae in the DGRP population. Each data point represents the intercept of the average GF larvae length and its corresponding mono-associated average length at Day 7 for each DGRP line. If genetic variation was the only factor influencing growth in both GF and mono-associated flies, the slope of the scatterplot should theoretically be 1 (Null hypothesis: slope = 1. $p < 0.0001$: the null hypothesis is therefore rejected. A linear standard curve with an unconstrained slope was used to fit the data).

(G–J) Hierarchical clustering (G: GF and I: mono-associated) and principal-component analyses (PCA) (H: GF and J: mono-associated) based on individual larvae transcriptome analyses show that the samples cluster more based on genotypes when germ-free (G and H, G: $P_{genotype} = 1.048 \times 10^{-8}$, H: $R^2_{Dim1} = 0.73$, $P_{genotype} = 7.81 \times 10^{-10}$, $R^2_{Dim2} = 0.72$, $P_{genotype} = 1.12 \times 10^{-9}$) than mono-associated (I and J, I: $P_{genotype} = 0.000263$, J: $R^2_{Dim1} = 0.42$, $P_{genotype} = 0.00017$, $R^2_{Dim2} = 0.31$, $P_{genotype} = 0.00269$). A scaled PCA using the genotype as categorical supplementary variable was performed. A hierarchical clustering on principle components (HCPC) was applied on the PCA results, and the trees were automatically cut based on inertia drop (Figure S2F). Both PCA and HCPC were performed with the R package FactoMineR on the voom corrected read counts. Correlations between the genotype variable and PCA dimensions or HCPC clusters were assessed by χ^2 tests. The dots represent the different samples according to genotype, and the empty squares are the calculated centers for each genotype.

(K) Gene set enrichment analysis based on the change in standard deviation of gene expression. Positive enrichment indicates gene sets that are enriched in the genes whose expression level variation increases in response to Lp^{WJL} mono-association. Negative gene sets are those that are enriched in the genes whose expression level variation decreases in response to Lp^{WJL} mono-association. The top four positively and negatively enriched sets are labeled. The genes whose expression levels are reduced by Lp^{WJL} mono-association predominantly act in chitin biosynthesis and morphogenesis (see also Figure S2).

variation in individual Lp^{WJL} mono-associated larvae with that of age-matched GF samples (Figures S2A). To minimize the size difference between the GF and mono-associated larvae to ensure sample homogeneity, we provided the GF larvae with 33% more yeast in the diet (more detailed description later) and analyzed the individual transcriptomes at an earlier time point (Day 4 post-embryonic development) where the size difference between the GF and mono-associated larvae is subtle. First, we observed that the transcriptomes moderately cluster by genotype and Lp^{WJL} status after batch effect correction (Figures S2B and S2C, Table S3). Specifically, samples from line 25,208, a "weak GF grower," showed the greatest transcriptomic changes and growth response to Lp^{WJL} association, whereas samples from line 25,210, a "strong GF grower," tend to cluster more based on genotype. Second, the overall transcriptomic changes associated with Lp^{WJL} presence corroborate several previous studies, including our own (Dobson et al., 2016; Erkosar et al., 2014). For example, genes involved in immune response and proteolysis, such as *LysB*, *PGRP-SC1a&b* are significantly up-regulated (Figure S2D). In addition, GO terms such as "immune response," "defense response," and "cellular component assembly involved in morphogenesis" are among the most up-regulated gene sets by mono-association (Figure S2E, top panel), and genes associated to "response to nutrient levels," "cellular response to starvation," and "tRNA modification" were down-regulated by Lp^{WJL} (Figure S2E, bottom panel). Therefore, both microbe sensing and nutrient adaptation drive the most significantly detected transcriptomic changes in mono-associated larvae.

Interestingly, we found that genotype was a stronger clustering driver for GF transcriptomes than for Lp^{WJL} mono-associated ones. When we added "genotype" as an illustrative variable in the principal component analysis based on bacterial presence, we observed that genotype has higher coefficients of correlation in the two first axes of variation in GF samples (compare Figures 1G versus 1I., and 1H. versus 1J. and S2F). These observations suggest that Lp^{WJL} can mask host genetic differences also at the transcriptomic level. Next, we compared the standard deviation (SD) of each expressed gene in both conditions and found that mono-association can either elevate or reduce expression variation in different gene sets (Figures S2G and S2H). Among the genes whose expression variation decreased the most upon Lp^{WJL} association are *Ssrp*, a member of the FACT chromatin complex (Saunders et al., 2003; Shimojima et al., 2003), and many cuticle-related proteins (Figure S2G, left panel), whereas for genes induced by Lp^{WJL}, such as Larval serum proteins (Lsp1s), more expression variation is detected (Figure S2G, right panel). This result suggests that mono-association does not indiscriminately reduce variation in the entire transcriptome, even though the GF transcriptomes tended to show an overall increase in expression variation (Figure S2H, red line), and this trend was more apparent in genes that were non-differentially expressed between the GF and mono-associated

conditions (Figure S2I, middle panel, gray lines). Finally, we found that genes whose expression variation was most decreased by Lp^{WJL} are enriched in developmental processes such as "body morphogenesis" and "cuticle development" (Figure 1K). These data reveal that Lp^{WJL} mono-association dampens genotype-dependent expression variation, especially of genes linked to developmental processes, which in turn may account for the ability of Lp^{WJL} to reduce larval size variation.

Lp^{WJL} Broadly Buffers Variation in Different Physical Fitness Traits in Genetically Diverse Populations

So far we have found that Lp^{WJL} reduces both phenotypic and transcriptional fluctuations during chronic under-nutrition, thus conferring a biological function that resembles various canonical buffering mechanisms that maintain phenotypic homogeneity by masking the effects of cryptic genetic variation (Mestek Boukhibar and Barkoulas, 2016; Posadas and Carthew, 2014; Rohner et al., 2013; Rutherford et al., 2007), despite the presence of a persistent nutritional stress signal. Since our studies insofar were conducted only in homozygous inbred DGRP lines, we sought to test if the observed buffering also operates in a population of genetically heterogeneous individuals. Therefore, based on their GF growth profile, we selected two DGRP strains from each end of the phenotypic extremes (Figures 1B and 1C, patterned pink and blue bars), established seven different inter-strains crosses, and compared the growth variation in the GF and mono-associated F_2 progenies (Figure S3A, Transparent Methods). As in the RNA-seq experiment, we also supplemented the GF larvae with 33% more yeast ($8g.L^{-1}$ versus $6g.L^{-1}$) to address two possible caveats: first, we wished to exclude that Lp^{WJL} might simply act as an additional inert source of nutrients. Several recent studies have demonstrated that live fly gut-associated symbionts can provide different micronutrients to the host, thus boosting growth and lifespan (Keebaugh et al., 2018; Wong et al., 2014; Yamada et al., 2015). Our previous findings demonstrate that the *Lp* symbionts need to be alive to assert their full beneficial impact in growth. For example, inoculating 1X living bacteria works far more efficiently to promote larval growth than adding three doses of 100X heat-inactivated bacteria within the first 7 days of development (Storelli et al., 2018). However, it is important to assess if increasing dietary yeast content can also reduce the variability in GF growth to the same extent as the gut bacteria, so that the observed buffering effect by the bacteria may be generally attributed to augmented "inert food effect," a somewhat trivial conclusion. Second, greater yeast content accelerates GF growth, thus allowing us to compare variation in size-matched GF and mono-associated larvae *en masse*, while minimizing the size and stage differences between the GF and mono-associated larvae. As GF larvae are growth-delayed and take longer to reach the same physical size compared with their mono-associated siblings, they can accumulate more developmental noise as a consequence of aberrantly protracted physiological responses, which in turn may contribute to higher phenotypic variation. In the same line of reasoning, at the same age, the faster developing mono-associated larvae have had less time to accumulate developmental noise and are closer to maturation than the germ-free larvae; thus, they can appear more uniform phenotypically, which may also account for less variability. To limit such bias imposed by the potential difference in developmental stage, we chose to augment the yeast content of the food for the GF larvae, and with the "boost" in GF growth, we compared the variances of growth when both GF and mono-associated larvae reach similar physical size during a comparable growth period.

In our initial testing trials, we found that the additional yeast invariably accelerated GF growth in different genetic backgrounds, sometimes to the same extent of the Lp^{WJL} presence (Figure S3C). However, when pooled based on dietary yeast content, the GF larvae that have received more yeast were longer but showed greater variation in lengths (Figure S3D). Moreover, in the genetically heterogeneous F_2 larvae, the CV and SD values tend to separate into two distinct groups, as driven by Lp^{WJL} presence (Figures 2A and S3B). Overall, the F_2 Lp^{WJL} mono-associated larvae were slightly longer, but their GF siblings varied more in length, regardless of yeast content or larval age (Figure S3E). In the size-matched pools (Figure 2A, purple bracket), GF size still fluctuated more than that of the Lp^{WJL} mono-associated siblings (Figure 2B), despite the fact that they were raised on a richer diet. Therefore, we first confirm that augmenting yeast content fails to recapitulate the same buffering effect mediated by living commensals. This is consistent with our previous observation that Lp-mediated transcriptomic buffering is readily visible, even if the GF transcriptomes are derived from larvae that have been raised on greater yeast quantities (Figures 1 and S2). More importantly, we conclude that phenotypic buffering by the gut microbe Lp^{WJL} indeed operates in a genetically diverse host population facing a nutritional challenge, hence qualifying the gut microbiota as a previously unappreciated buffering agent of cryptic genetic variation.

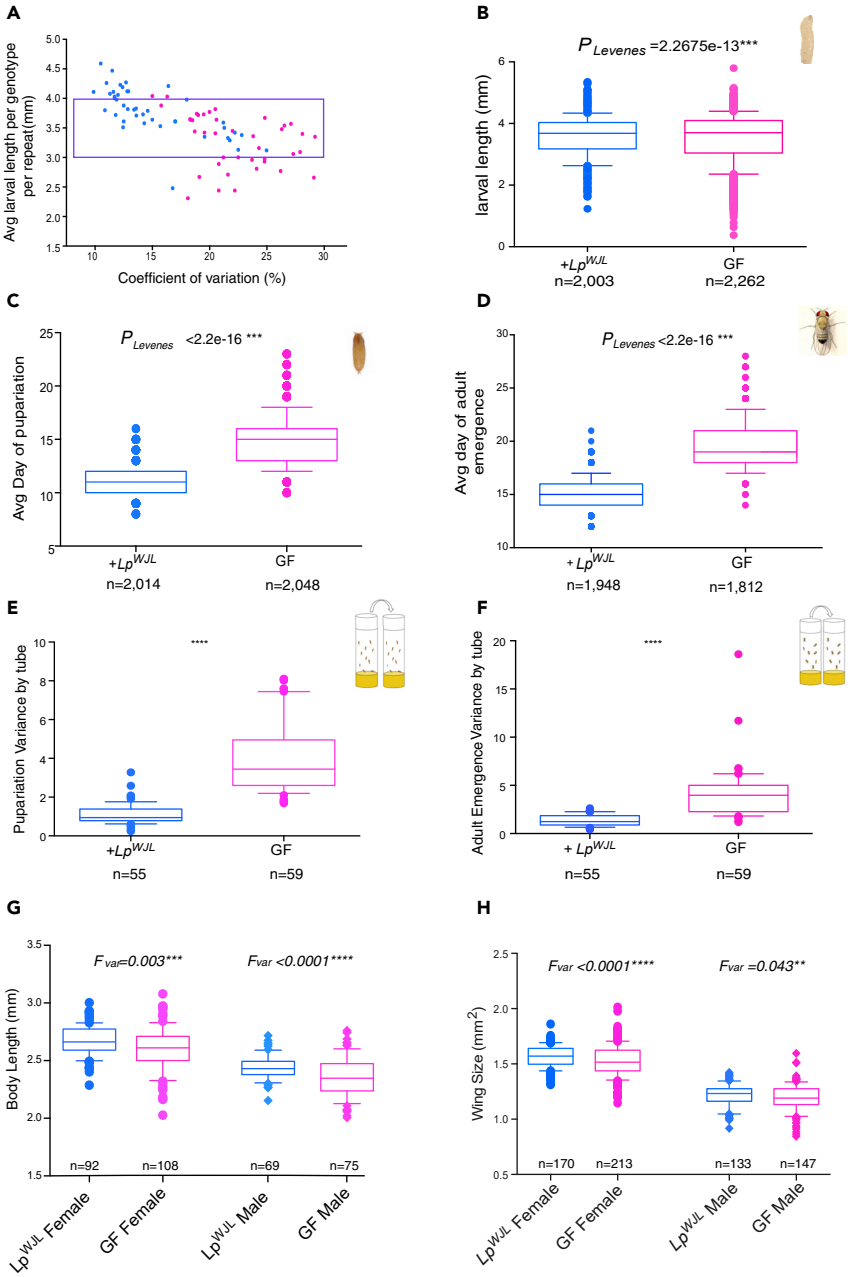

Figure 2. In the Genetically Diverse DGRP F_2 Population, Lp^{WJL} Reduces Variation in Different Physical Fitness Traits

(A) A scatterplot showing how coefficient of variation (CV) changes as a function of larval length and how such change differs in the DGRP F_2 GF (pink) and Lp^{WJL} mono-associated (blue) populations (see Figure S3A and Methods for detailed schemes). Each data point represents the intercept of a CV value and its corresponding average larval length in a particular cross. Each CV, SD, and average value was derived from larvae measurements gathered from at least three biological replicates from either GF or Lp^{WJL} mono-associated conditions. Each replicate contains 10–40 larvae. Based on multivariate ANOVA analysis, the factors affecting variants in this plot are: larval age* ($p = 0.053$), bacterial presence***($p = 3.02 \times 10^{-6}$), and larval length ($p = 8.27 \times 10^{-15}$***). The purple bracket indicates the arbitrarily selected experiments where the average larval length for each cross falls between 3 and 4 mm for size-matching purpose.

(B) The average larval length of the F_2 progeny pooled from experiments demarcated by the purple bracket in Figure 2A. The average size is perfectly matched (GF Avg Length = 3.522mm, Lp^{WJL} Avg Length = 3.582mm, $p = 0.857^{ns}$, Mann-Whitney test), whereas the GF population exhibits greater variation than the Lp^{WJL} mono-associated population ($Var_{GF} = 0.642$, $CV_{GF} = 22.8\%$, $Var_{Lp} = 0.427$, $CV_{Lp} = 18.3\%$).

Figure 2. *Continued*

(C) Variance and mean comparisons for the average day of pupariation for individual larva in the F_2 GF and mono-associated populations. (Difference in mean $p < 0.0001$***, Mann-Whitney test, $Var_{GF} = 2.42$, $Var_{Lp} = 1.22$).

(D) Variance comparison for average day of adult emergence in the F_2 GF and mono-associated populations (Difference in mean $p < 0.0001$***, $Var_{Lp} = 1.84$, $Var_{GF} = 5.27$).

(E) Box plots comparing the variances of pupariation derived from each tube containing approximately 40 larvae. The average variance per tube for the GF population = 3.99; the average variance per tube for the Lp^{WJL}-associated population = 1.12. $Var_{Lp} = 0.54$, $Var_{GF} = 1.76$. Note that these values are the "variance of variances."

(F) Box plots comparing the variances for adult emergence from each tube containing approximately 40 larvae (difference in mean $p < 0.0001$***). The average variance per tube for the GF population = 4.06; the average variance per tube for the Lp^{WJL} associated population = 1.34. For "variance of the variances," $Var_{Lp} = 1.33$, $Var_{GF} = 4.2$.

(G and H) In both male (lozenge) and female (circle) adults, the variances in body size (G the difference in mean body length: for females, $p = 0.003$***, for males, $p < 0.0001$****) and wing size (H, the difference in mean wing area for females, $p < 0.0001$**** for males, $p = 0.043$**) are greater in the GF population than in the mono-associated population. The adult datasets presented in Figures 2G and 2H and in S3G and S3H take on normal distribution by D'Agostino and Pearson omnibus normality test, F variances are therefore calculated and compared. Data are represented as mean and 10–90 percentile in all panels.

During chronic under-nutrition, Lp^{WJL} sustains growth rate as effectively as an entire gut associated commensal community (Storelli et al., 2011). We thus wondered if a natural and more complex gut-associated community can also buffer growth variation like Lp^{WJL}. To address this question, we rendered a population of wild flies collected in a nearby garden germ-free, and re-associated them with their own fecal microbial community (Tefit et al., 2018). In three of four experimental repeats, growth variation is significantly reduced in the larval population fed on food inoculated with their parents' fecal microbes (Figure S3F and data not shown), and the cumulative CV and variances derived from each food cap were significantly higher in the GF population (Figures S3G and S3H). This suggests that the gut-associated microbial community of wild flies indeed decreases growth variation of a natural *Drosophila* population. However, since the wild-derived microbes did not consistently buffer larval growth, probably due to the difficulty to precisely control the quantity and composition of the inoculated fecal microbiota, we returned to the mono-association model for subsequent studies.

If the observed growth variation in GF larvae indeed reflects the "unleashing" of the host's genetic potential due to the loss of a buffering mechanism provided by gut microbes, then we posit that other physical fitness traits in a fertile surviving GF population should in principle also exhibit greater phenotypic variation. We therefore examined the variances in pupariation timing and adult emergence in the F_2 progeny of the inter-DGRP strain crosses (Figure S3A). First, individual GF larvae pupariated and eclosed later, but the variances in the pooled data were greater than that of mono-associated counterparts (Figures 2C and 2D); from each vial containing an equal number of larvae, the variances of pupariation and eclosion were also greater in the GF samples (Figures 2E and 2F). Therefore, both inter-individual and among-population variances in developmental timing and adult emergence are reduced upon mono-association. Lastly, GF adults were slightly shorter (Figure 2F); the sizes of representative organs, expressed as area of the eye and the wing, were also smaller, yet the variances in these traits were greater (Figures 2H and S3I). Furthermore, the wing/body-length allometric slopes remained unaltered, but the individual GF values were more dispersed along the slope (Figures S3J and S3K); when taken as a ratio (wing length/body-length), the variance was greater in the GF flies (Figure S3L). These observations indicate that gut microbes, represented by Lp^{WJL}, confer phenotypic homogeneity in various physical fitness traits in a genetically diverse host population under nutritional stress.

Lp^{WJL} Conveys Robustness in Organ-Patterning under Nutritional Stress

We have thus far shown that Lp^{WJL} association confers transcriptomic stability and phenotypic constancy to the developing host facing nutritional stress, in a fashion that is reminiscent of the host's own genetic buffering mechanism. For example, reducing Hsp90 activity has been shown to increase organ size variation in both plants and animals (Queitsch et al., 2002; Rohner et al., 2013; Rutherford and Lindquist, 1998). Moreover, compromising Hsp90 can lead to morphological aberrations that are otherwise "hidden" (Rutherford and Lindquist, 1998). Similarly, we also found that a significant fraction of the GF F_2 flies bore aberrant wing patterns such as missing margins, incomplete vein formations, and ectopic vein tissue (Figure 3A). The incidence of wing anomalies differed according to the genotype, and females were more affected than males (Figure 3B). In contrast, the most visible "defect" in their Lp^{WJL} associated siblings, if any, were rare and hardly discernable (Figures 3A and S4A). Furthermore, gross patterning anomalies were absent in the viable adults from the GF parental homozygous strains or in

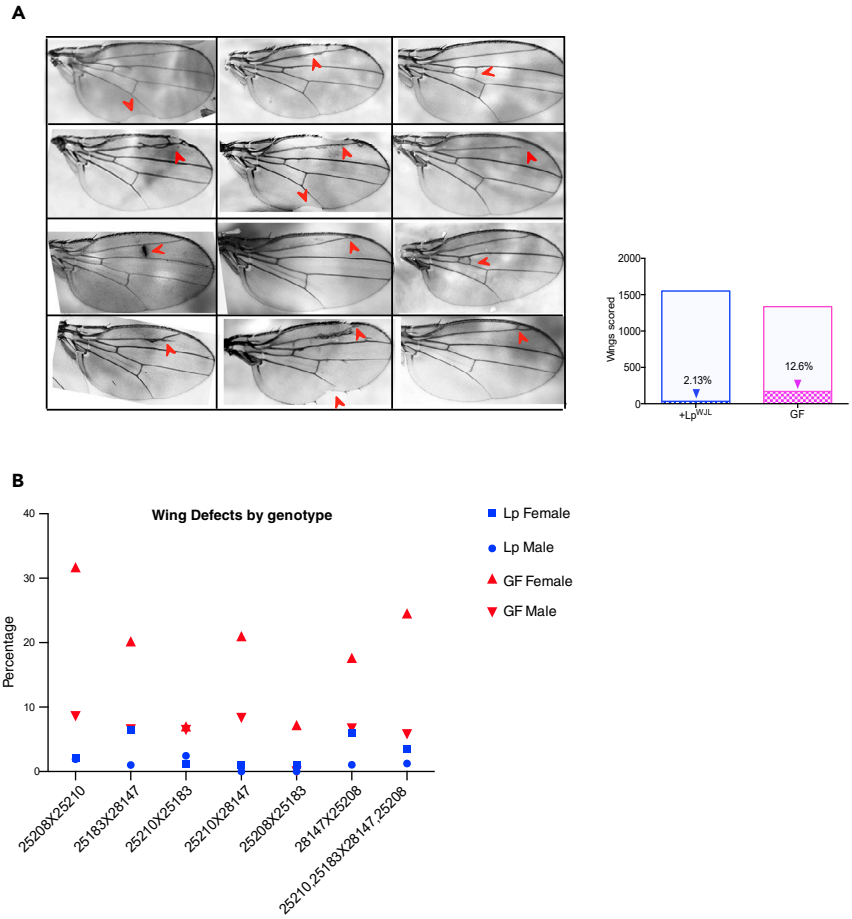

Figure 3. In the DGRP F_2 Progeny, Lp^{WJL} Association Provides Robustness in Wing Developmental Patterning

(A) A compilation of representative images illustrating wing patterning anomalies in the GF DGRP F_2 progeny, indicated by red arrows. The number of such patterning anomalies are compiled together for GF and Lp^{WJL} mono-associated flies ($\chi 2$ test, $p < 0.0001$***, N_{Lp} = 1,551 N_{GF} = 1,335), and the percentage of defects are indicated inside each bar.

(B) The incidence of wing patterning defects separated by F_2 genotypes. The y axis denotes the percentage of wings with aberrant patterning as represented in Figure 3A.

F_2 adults reared on a standard diet (data not shown), supporting the notion that the fly gut-associated commensals likely act as a canalization mechanism by suppressing the contribution of cryptic genetic variation to developmental phenotypes in the presence of nutritional stress. Organ patterning is a robust process; changes in nutrition, humidity, temperature, and crowding can alter the final adult body and wing size; yet wing patterning is usually invariant and reproducible (Mirth and Shingleton, 2012). Surprisingly, we found that, in GF flies, constant nutritional stress can in fact unveil the effects of preexisting "silent" mutations that manifest themselves as visible wing patterning anomalies. Furthermore, as the patterning defects appear only in nutritionally challenged F_2 flies devoid of their gut-associated commensals, we conclude that these defects reflect a breach of the canalization process during developmental patterning when the hidden effects of genetic variants are unlocked (Waddington, 1959) and the gut-associated symbionts buffer the effects of these otherwise seemingly "neutral" variants to confer robustness to the canalized process of organ patterning.

Compromising ROS Activity Impairs the Buffering Capacity of Lp^{WJL} without Affecting Bacterial Growth

The wing anomalies in the GF F_2 progeny highly resemble the phenotypes reported by Santabarbara-Ruiz et al., who blocked ROS by feeding the larvae with antioxidants, such as *N*-acetylcysteine (NAC), and induced regeneration defects in the wing (Santabarbara-Ruiz et al., 2015). NAC is a widely used and safe antioxidant that has been repeatedly used to block ROS without adversely affecting adult feeding behavior

(Atkuri et al., 2007; Bailey et al., 2015; Santabarbara-Ruiz et al., 2015; Sun et al., 2012). We therefore repeated the DGRP F_2 cross experiment with an additional condition by mixing the antioxidant molecule NAC in the diet of mono-associated flies. First, germ-free larvae fed on NAC tended to be small, yet the variance in their size is comparable with that of mono-associated flies fed with NAC and of germ-free flies never exposed to NAC (Figure S4B). However, over 95% of NAC-fed germ-free larvae failed to pupariate, making it impossible to assess variances in developmental timing and adult traits. Furthermore, NAC feeding did not compromise bacterial growth (Figure S4C) but significantly diminished the buffering capacity of Lp^{WJL} (Figure 4). Specifically, variation in larval size (Figure 4A), developmental timing (Figures 4B and 4D), and adult emergence (Figures 4C and 4E) were significantly increased in NAC-fed larvae mono-associated with Lp^{WJL}, to a level similar to or even higher than that in GF larvae. Wing patterning anomalies were also unmasked (Figure 4F). Therefore, blocking ROS activity through NAC feeding suppresses the genetic buffering effect mediated by the gut bacteria.

DISCUSSION

Here we show that a single *Drosophila* gut commensal strain Lp^{WJL} functionally resembles a general buffer mechanism that safeguards the host's genetic potential and confers developmental robustness in times of nutritional stress. This conclusion emerged from our analyses in different genetic contexts, such as the DGRP lines, the RNAi knock-down crosses, and the heterozygous F2 crosses, in which we observed that Lp^{WJL} mono-associated flies not only grow better than their germ-free counter parts but also show less variation in transcriptional and phenotypic traits related to growth and maturation. Microbial buffering also operates in wild-derived flies associated with their endogenous gut communities, which implies that such buffering may be a universal feature of many beneficial microbes. In *Drosophila*, nutritional mutualism with commensals is inconstant and volatile by nature (Broderick et al., 2014; Storelli et al., 2018; Wong et al., 2013), in that the gut community composition highly varies among individuals and along the life stages of each individual. Consequently, the rapid acquisition or loss of particular gut community members can alter the functionality and capacity of the gut-associated symbionts, which in turn affects how the developing host population adjusts its phenotypic range to adapt to the changing environment during their life. Furthermore, under nutritional stress, genetically diverse fly populations devoid of their gut microbes manifest wing patterning defects that are masked by the presence of a gut microbe. The action of genetic buffering by the gut commensal bacteria therefore maintains organ patterning robustness for the developing population while facing nutritional stress.

Gut commensals stimulate host ROS production, which consequently elicits diverse physiological consequences. Jones et al. previously reported that acute exposure to *Lactobacillus plantarum* stimulates the *dNox*-dependent production of ROS in larval enterocytes and subsequently increases the expression of genes involved in the Nrf2-mediated cyto-protection program (Jones et al., 2013, 2015). In adult flies, *Lp*-derived lactic acid stimulates ROS production and leads to shortened lifespan, which is rescued by blocking ROS with NAC feeding (Iatsenko et al., 2018). Therefore, the microbial regulation of ROS is highly complex and seems to mediate antagonistic outcomes depending on host life-stages. Our results further add to such complexity. We identified an unexpected role of ROS in mediating microbial buffering of host phenotypic variance. Blocking ROS in germ-free flies leads to maturation failure, but without further increasing variation in larval growth. This result suggests that ROS-mediated microbial buffering of growth is separable from its involvement in metamorphosis. Future explorations are required to reconcile how ROS activity can be integrated into the molecular dialogue between the host and its gut microbiome to maintain robustness during development.

A recent study by Elgart et al. showed that, when raised on standard food, the wild-type, axenic embryonic transcriptome showed accelerated maternal-zygotic-transition (MZT) and a shortened period of embryogenesis. Moreover, four *Drosophila* strains, each bearing a single, heterozygous genetic mutation manifested greater variance in pupariation timing in the germ-free progeny than in their axenic parents (Elgart et al., 2016). Whether the accelerated MZT in germ-free, wild-type embryos can account for a mechanism inducing greater larval maturation variability in the mutant progeny remains to be elucidated. However, the fact that in axenic flies, hidden phenotypic variation is revealed in the next generation is consistent with our finding that microbial buffering acts through unmasking CGVs. As greater phenotypic, transcriptomic variation and organ patterning anomaly are only observed in germ-free flies under nutritional stress, our results indicate that microbial buffering may be a natural outcome of long-term co-evolution with the host under strong selection pressure. Therefore, we propose that the facultative gut commensals not only increase the host's fitness in a stressful environment during its lifetime but also enable its evolutionary adaptation by preserving the host's CGVs in the long run.

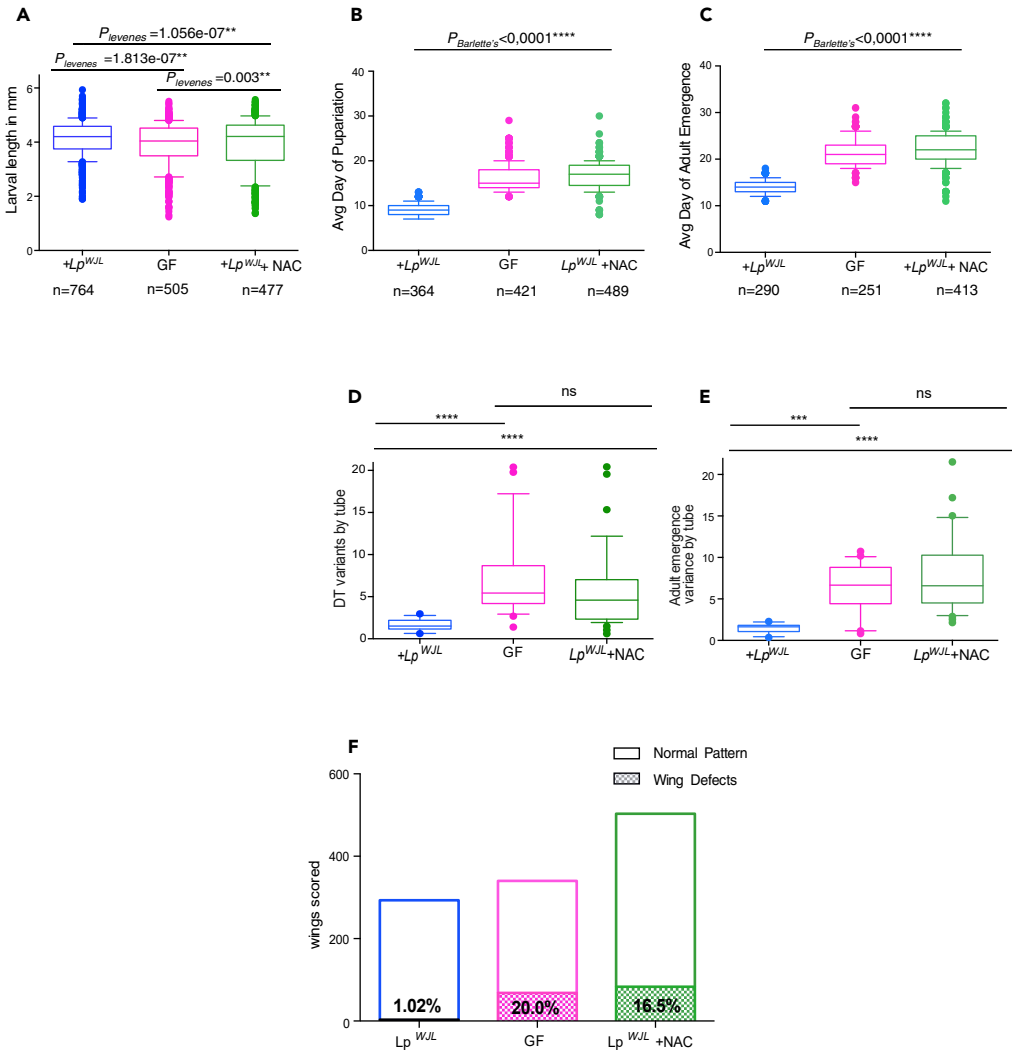

Figure 4. Blocking ROS Activity by N-acetylcysteine (NAC) Compromises the Lp^{WJL} Buffering Capacity

(A) In the DGRP F_2 progeny, feeding Lp^{WJL} mono-associated animals with food supplemented with NAC increases the variances in size-matched larvae. Average Lp larval size: 4.08mm; average GF larval size: 3.83mm; average Lp^{WJL} + NAC larval size: 3.94mm. There is no size difference between GF and NAC-treated flies associated with Lp^{WJL}, p = 0.064. CV_{Lp} = 15.8%, CV_{GF} = 20.8%; CV_{Lp+NAC} = 24.0%.

(B and C) NAC treatment to the Lp-associated animals also increases the variances of pupariation (B) and adult emergence (C). The average day to become a pupa for Lp^{WJL} mono-associated larva: Day 8.9 (Var = 2.13); for a GF larva: Day 16.1 (Var = 8.27); for a NAC-treated, mono-associated larva: Day 16.8 (Var = 8.36). The average day for an Lp^{WJL} mono-associated adult to emerge is: Day14.1 (Var = 2.08), for a GF adult: Day 21 (Var = 8.3), and for an NAC-treated, mono-associated adult: Day 21.7 (Var = 11.3).

(D and E) NAC treatment to the Lp^{WJL} mono-associated animals also increases the among-population variances of pupariation and adult emergence. Each data point represents the variance calculated based on the average day of pupariation (D) or adult emergence (E) from each tube housing approximately 40 animals.

(F) Morphological defects in the wings are also significantly increased in NAC-treated mono-associated adults ($\chi 2$ test, p < 0.0001***) pink: GF (N = 340); Blue: +Lp^{WJL} (N = 293), Green: + Lp^{WJL} + NAC (N = 503). Data are represented as mean and 10–90 percentile in all panels.

Limitations of the Study

We have observed the effects of microbial buffering in a genetically diverse population, making the search for "buffering genes" a challenge, as classic genetic screens in *Drosophila* do not apply. By the same token, to alter ROS activity in the genetically diverse F2s, we had to resort to NAC treatment, which is a conventional and widely accepted approach to block ROS in the broad literature. We obtained the expected

results, namely, the buffering capacity of *Lactobacillus plantarum* is compromised, but future QTL studies are required confirm the role of the ROS pathway and identify genes and variants affected by such microbial buffering activities.

METHODS

All methods can be found in the accompanying Transparent Methods supplemental file.

SUPPLEMENTAL INFORMATION

Supplemental Information can be found online at https://doi.org/10.1016/j.isci.2019.07.048.

ACKNOWLEDGMENTS

We would like to thank Benjamin Prud'homme and colleagues at ENS de Lyon and EPFL for their critical reading of the manuscript and valuable suggestions, the ArthroTools platform of the SFR Biosciences (UMS3444/US8) for the fly equipment and facility, and the Bloomington Stock Centre and VDRC for fly lines. This work was supported by an international collaborative grant through the French "Agence Nationale de la Recherche" and the "Fond National Suisse pour la Recherche" (ANR-15-CE14-0028-01) awarded to F.L. and B.D., an ERC starting grant (FP7/2007-2013-N_309704) awarded to F.L., a SystemsX.ch (AgingX) Grant awarded to B.D., and Institutional Support by the EPFL (B.D.). C.-E.I. was funded by a Ph.D. fellowship from the Rhone-Alps region. F.L. is supported by the Finovi, FRM, and FSER foundations and the EMBO Young Investigator Program. M.B.-S., M.F., M.L., and B.D. were supported by AgingX (SystemsX.ch) and/or Institutional Support by the EPFL.

AUTHOR CONTRIBUTIONS

D.M., M.B.-S., B.D., and F.L. conceived the project and designed the experiments; D.M. and C.-E.I. conducted all fly-related experiments; M.B.-S. and M.L. conducted the GWAS analysis; M.B.-S, M.F., and V.B. prepared the libraries and conducted single-larvae transcriptome analyses. P.J. conducted the multivariate statistical analyses; G.S., has identified the effect of NAC on *Lp*-mediated larval phenotypes. D.M., M.B.-S., B.D., and F.L. analyzed the data. D.M. drafted the manuscript, D.M., M.B.-S, B.D., and F.L revised the paper and wrote the final draft together.

DECLARATION OF INTERESTS

The authors declare no competing financial interests. Correspondence and requests for materials should be addressed to francois.leulier@ens-lyon.fr or bart.deplancke@epfl.ch.

Received: December 13, 2018
Revised: April 25, 2019
Accepted: July 30, 2019
Published: September 27, 2019

REFERENCES

Alpern, D., Gardeux, V., Russeil, J., Mangeat, B., Meireles-Filho, A., Breysse, R., Hacker, D., and Deplancke, B. (2019). BRB-seq: ultra-affordable high-throughput transcriptomics enabled by bulk RNA barcoding and sequencing. Genome Biol. *20*, https://doi.org/10.1186/s13059-019-1671-x.

Atkuri, K.R., Mantovani, J.J., Herzenberg, L.A., and Herzenberg, L.A. (2007). N-Acetylcysteine–a safe antidote for cysteine/glutathione deficiency. Curr. Opin. Pharmacol. *7*, 355–359.

Bailey, A.P., Koster, G., Guillermier, C., Hirst, E.M., MacRae, J.I., Lechene, C.P., Postle, A.D., and Gould, A.P. (2015). Antioxidant role for lipid droplets in a stem cell Niche of Drosophila. Cell *163*, 340–353.

Broderick, N.A., Buchon, N., and Lemaitre, B. (2014). Microbiota-induced changes in drosophila melanogaster host gene expression and gut morphology. MBio *5*, e01117–01114.

Brucker, R.M., and Bordenstein, S.R. (2013). The hologenomic basis of speciation: gut bacteria cause hybrid lethality in the genus Nasonia. Science *341*, 667–669.

Clemente, J.C., Ursell, L.K., Parfrey, L.W., and Knight, R. (2012). The impact of the gut microbiota on human health: an integrative view. Cell *148*, 1258–1270.

Dobson, A.J., Chaston, J.M., and Douglas, A.E. (2016). The Drosophila transcriptional network is structured by microbiota. BMC Genomics *17*, 975.

Elgart, M., Stern, S., Salton, O., Gnainsky, Y., Heifetz, Y., and Soen, Y. (2016). Impact of gut microbiota on the fly's germ line. Nat. Commun. *7*, 11280.

Erkosar, B., Defaye, A., Bozonnet, N., Puthier, D., Royet, J., and Leulier, F. (2014). Drosophila microbiota modulates host metabolic gene expression via IMD/NF-kappaB signaling. PLoS One *9*, e94729.

Flatt, T. (2005). The evolutionary genetics of canalization. Q. Rev. Biol. *80*, 287–316.

Gilbert, J.A., and Neufeld, J.D. (2014). Life in a world without microbes. PLoS Biol. *12*, e1002020.

Gilbert, S.F. (2014). Symbiosis as the way of eukaryotic life: the dependent co-origination of the body. J. Biosci. *39*, 201–209.

Huang, W., Massouras, A., Inoue, Y., Peiffer, J., Ramia, M., Tarone, A.M., Turlapati, L., Zichner, T., Zhu, D., Lyman, R.F., et al. (2014). Natural variation in genome architecture among 205 *Drosophila melanogaster* Genetic Reference Panel lines. Genome Res. *24*, 1193–1208.

Iatsenko, I., Boquete, J.P., and Lemaitre, B. (2018). Microbiota-derived lactate activates production of reactive oxygen species by the intestinal NADPH oxidase Nox and shortens Drosophila lifespan. Immunity *49*, 929–942.e5.

Jones, R.M., Desai, C., Darby, T.M., Luo, L., Wolfarth, A.A., Scharer, C.D., Ardita, C.S., Reedy, A.R., Keebaugh, E.S., and Neish, A.S. (2015). Lactobacilli modulate epithelial cytoprotection through the Nrf2 pathway. Cell Rep. *12*, 1217–1225.

Jones, R.M., Luo, L., Ardita, C.S., Richardson, A.N., Kwon, Y.M., Mercante, J.W., Alam, A., Gates, C.L., Wu, H., Swanson, P.A., et al. (2013). Symbiotic lactobacilli stimulate gut epithelial proliferation via Nox-mediated generation of reactive oxygen species. EMBO J. *32*, 3017–3028.

Keebaugh, E.S., Yamada, R., Obadia, B., Ludington, W.B., and Ja, W.W. (2018). Microbial quantity impacts Drosophila nutrition, development, and lifespan. iScience *4*, 247–259.

Kim, E.K., Park, Y.M., Lee, O.Y., and Lee, W.J. (2013). Draft genome sequence of Lactobacillus plantarum strain WJL, a Drosophila gut symbiont. Genome Announc. *1*, e00937–13.

Lehner, B. (2013). Genotype to phenotype: lessons from model organisms for human genetics. Nat. Rev. Genet. *14*, 168–178.

Ma, D., and Leulier, F. (2018). The importance of being persistent: the first true resident gut symbiont in Drosophila. PLoS Biol. *16*, e2006945.

Mackay, T.F., Richards, S., Stone, E.A., Barbadilla, A., Ayroles, J.F., Zhu, D., Casillas, S., Han, Y., Magwire, M.M., Cridland, J.M., et al. (2012). The *Drosophila melanogaster* genetic reference panel. Nature *482*, 173–178.

Mestek Boukhibar, L., and Barkoulas, M. (2016). The developmental genetics of biological robustness. Ann. Bot. *117*, 699–707.

Mirth, C.K., and Shingleton, A.W. (2012). Integrating body and organ size in Drosophila: recent advances and outstanding problems. Front. Endocrinol. (Lausanne) *3*, 49.

Obadia, B., Keebaugh, E.S., Yamada, R., Ludington, W.B., and Ja, W.W. (2018). Diet influences host-microbiota associations in Drosophila. Proc. Natl. Acad. Sci. U S A *115*, E4547–E4548.

Pais, I.S., Valente, R.S., Sporniak, M., and Teixeira, L. (2018). Drosophila melanogaster establishes a species-specific mutualistic interaction with stable gut-colonizing bacteria. PLoS Biol. *16*, e2005710.

Posadas, D.M., and Carthew, R.W. (2014). MicroRNAs and their roles in developmental canalization. Curr. Opin. Genet. Dev. *27*, 1–6.

Queitsch, C., Sangster, T.A., and Lindquist, S. (2002). Hsp90 as a capacitor of phenotypic variation. Nature *417*, 618–624.

Rohner, N., Jarosz, D.F., Kowalko, J.E., Yoshizawa, M., Jeffery, W.R., Borowsky, R.L., Lindquist, S., and Tabin, C.J. (2013). Cryptic variation in morphological evolution: HSP90 as a capacitor for loss of eyes in cavefish. Science *342*, 1372–1375.

Rutherford, S., Hirate, Y., and Swalla, B.J. (2007). The Hsp90 capacitor, developmental remodeling, and evolution: the robustness of gene networks and the curious evolvability of metamorphosis. Crit. Rev. Biochem. Mol. Biol. *42*, 355–372.

Rutherford, S.L., and Lindquist, S. (1998). Hsp90 as a capacitor for morphological evolution. Nature *396*, 336–342.

Santabarbara-Ruiz, P., Lopez-Santillan, M., Martinez-Rodriguez, I., Binagui-Casas, A., Perez, L., Milan, M., Corominas, M., and Serras, F. (2015). ROS-induced JNK and p38 signaling is required for unpaired cytokine activation during Drosophila regeneration. PLoS Genet. *11*, e1005595.

Saunders, A., Werner, J., Andrulis, E.D., Nakayama, T., Hirose, S., Reinberg, D., and Lis, J.T. (2003). Tracking FACT and the RNA polymerase II elongation complex through chromatin in vivo. Science *301*, 1094–1096.

Shimojima, T., Okada, M., Nakayama, T., Ueda, H., Okawa, K., Iwamatsu, A., Handa, H., and Hirose, S. (2003). Drosophila FACT contributes to Hox gene expression through physical and functional interactions with GAGA factor. Genes Dev. *17*, 1605–1616.

Shin, S.C., Kim, S.H., You, H., Kim, B., Kim, A.C., Lee, K.A., Yoon, J.H., Ryu, J.H., and Lee, W.J. (2011). Drosophila microbiome modulates host developmental and metabolic homeostasis via insulin signaling. Science *334*, 670–674.

Sommer, F., and Backhed, F. (2013). The gut microbiota–masters of host development and physiology. Nat. Rev. Microbiol. *11*, 227–238.

Storelli, G., Defaye, A., Erkosar, B., Hols, P., Royet, J., and Leulier, F. (2011). Lactobacillus plantarum promotes Drosophila systemic growth by modulating hormonal signals through TOR-dependent nutrient sensing. Cell Metab. *14*, 403–414.

Storelli, G., Strigini, M., Grenier, T., Bozonnet, L., Schwarzer, M., Daniel, C., Matos, R., and Leulier, F. (2018). Drosophila perpetuates nutritional mutualism by promoting the fitness of its intestinal Symbiont *Lactobacillus plantarum*. Cell Metab. *6*, 362–377.

Sun, X., Komatsu, T., Lim, J., Laslo, M., Yolitz, J., Wang, C., Poirier, L., Alberico, T., and Zou, S. (2012). Nutrient-dependent requirement for SOD1 in lifespan extension by protein restriction in *Drosophila melanogaster*. Aging Cell *11*, 783–793.

Tefit, M.A., Gillet, B., Joncour, P., Hughes, S., and Leulier, F. (2018). Stable association of a Drosophila-derived microbiota with its animal partner and the nutritional environment throughout a fly population's life cycle. J. Insect Physiol. *106* (Pt 1), 2–12.

Waddington, C.H. (1959). Canalization of development and genetic assimilation of acquired characters. Nature *183*, 1654–1655.

Wagner, A. (2007). Robustness and Evolvability in Living Systems, Paperback edn (Princeton University Press).

Wong, A.C., Chaston, J.M., and Douglas, A.E. (2013). The inconstant gut microbiota of Drosophila species revealed by 16S rRNA gene analysis. ISME J. *7*, 1922–1932.

Wong, A.C., Dobson, A.J., and Douglas, A.E. (2014). Gut microbiota dictates the metabolic response of Drosophila to diet. J. Exp. Biol. *217*, 1894–1901.

Yamada, R., Deshpande, S.A., Bruce, K.D., Mak, E.M., and Ja, W.W. (2015). Microbes promote amino acid harvest to rescue undernutrition in Drosophila. Cell Rep. *10*, 865–872.

ISCI, Volume *19*

Supplemental Information

Commensal Gut Bacteria Buffer the Impact of Host Genetic Variants on *Drosophila* Developmental Traits under Nutritional Stress

Dali Ma, Maroun Bou-Sleiman, Pauline Joncour, Claire-Emmanuelle Indelicato, Michael Frochaux, Virginie Braman, Maria Litovchenko, Gilles Storelli, Bart Deplancke, and François Leulier

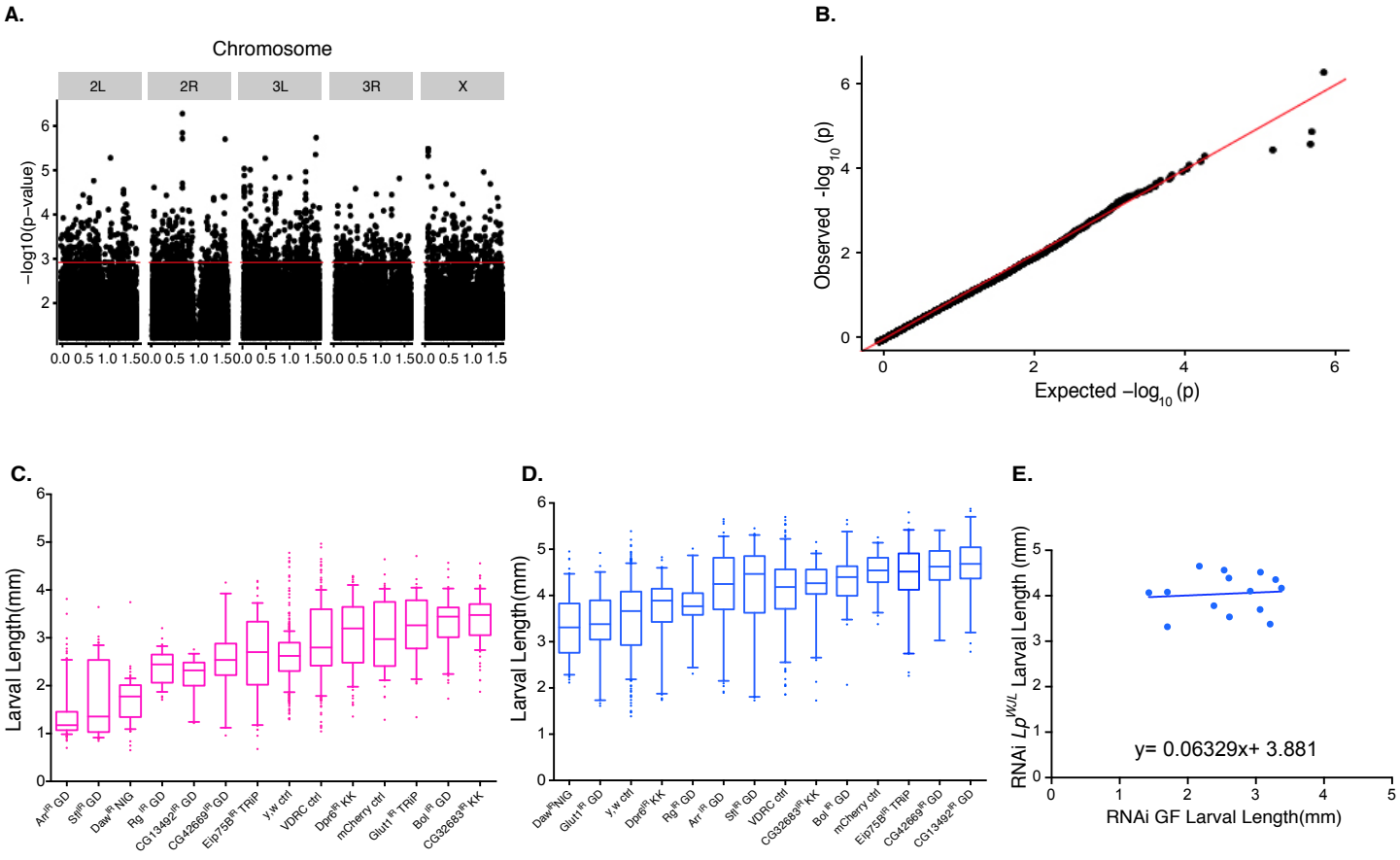
A.
Chromosome
2L
2R
3L
3R
X
−log10(p−value)
B.
Observed -log10 (p)
Expected –log10 (p)
C.
Larval Length(mm)
D.
Larval Length(mm)
E.
RNAi Lpwk/L Larval Length (mm)
y= 0.06329x+ 3.881
RNAi GF Larval Length(mm)

Figure S1

Figure S1. GWAS discovery of the growth promotion effect by *Lp*^{WJL} unexpectedly unveils the microbial buffering capacity in different host genetic backgrounds. Related to Figure 1

A). Manhattan plot of the GWAS performed on the average larval length fold change per DGRP line. We used the DGRP2 website for the association analysis. (http://dgrp2.gnets.ncsu.edu/)(Huang et al., 2014; Mackay et al., 2012).

B). Quantile-Quantile plot of the GWAS results.

C). and D). Box and whiskers plots illustrating the effect of RNAi knockdown on larval length on day 7 AEL. Each bar represents the average length from pooled 3-5 biological replicates from either condition, with 15-40 larvae in each replicate. **C:** GF. **D:** *Lp*^{WJL}. Three different control knockdowns were used: one control fly strain recommended by VDRC for RNAi constructs obtained from VDRC, one control strain (against mCherry) recommended by the Harvard TRiP collection, and the *y,w* strain from Bloomington. All control and RNAi strains were crossed to *y,w;; tubulin*-GAL80^{ts} ,*daugtherless*-GAL4. "GD" refers to the VDRC RNAi GD collection. "KK" refers to the VDRC RNAi KK collection. For specific genotypes, refer to Material and Methods.

E). *Lp*^{WJL} also buffers growth differences in the RNAi knock-down experiments for each of the candidate genes. Each data point represents the intercept of the average GF length and its corresponding mono-associated average larval length on Day 7 for each RNAi knockdown experiment. (Null hypothesis: Slope =1. *P=0.0008* , the null hypothesis is therefore rejected). These data points were fitted into an unconstraint model. For specific genotypes, we refer to Table 2 and Methods. Data are represented as mean and 10-90 percentile in all panels.

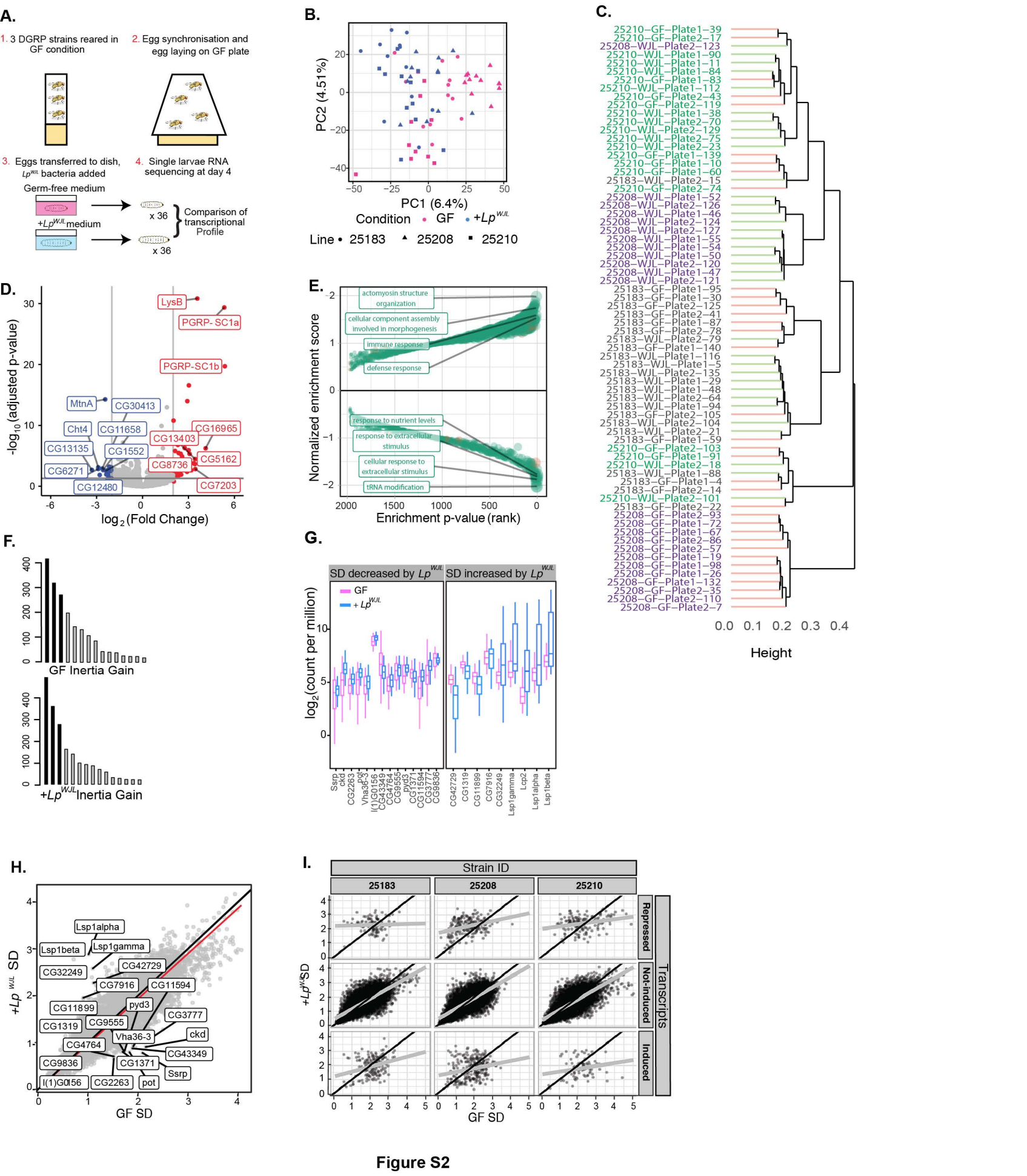
A.
1. 3 DGRP strains reared in GF condition
2. Egg synchronisation and egg laying on GF plate
3. Eggs transferred to dish, Lp^WJL bacteria added
4. Single larvae RNA sequencing at day 4
Germ-free medium
+Lp^WJL medium
x 36
x 36
Comparison of transcriptional Profile
B.
PC2 (4.51%)
PC1 (6.4%)
Condition GF +Lp^WJL
Line 25183 25208 25210
C.
25210–GF–Plate1–39
25210–GF–Plate2–17
25208–WJL–Plate2–123
25210–WJL–Plate1–90
25210–WJL–Plate1–11
25210–WJL–Plate1–84
25210–GF–Plate1–83
25210–WJL–Plate1–112
25210–GF–Plate2–43
25210–GF–Plate2–119
25210–WJL–Plate1–38
25210–WJL–Plate2–70
25210–WJL–Plate2–129
25210–WJL–Plate2–75
25210–WJL–Plate2–23
25210–GF–Plate1–139
25210–GF–Plate1–10
25210–GF–Plate1–60
25183–WJL–Plate2–15
25210–GF–Plate2–74
25208–WJL–Plate1–52
25208–WJL–Plate2–126
25208–WJL–Plate1–46
25208–WJL–Plate2–124
25208–WJL–Plate2–127
25208–WJL–Plate1–55
25208–WJL–Plate1–54
25208–WJL–Plate1–50
25208–WJL–Plate2–120
25208–WJL–Plate1–47
25208–WJL–Plate2–121
25183–GF–Plate1–95
25183–GF–Plate1–30
25183–GF–Plate2–125
25183–GF–Plate2–41
25183–GF–Plate1–87
25183–GF–Plate2–78
25183–WJL–Plate2–79
25183–GF–Plate1–140
25183–WJL–Plate1–116
25183–WJL–Plate1–5
25183–WJL–Plate2–135
25183–WJL–Plate1–29
25183–WJL–Plate1–48
25183–WJL–Plate2–64
25183–WJL–Plate1–94
25183–GF–Plate2–105
25183–WJL–Plate2–104
25183–WJL–Plate2–21
25183–GF–Plate1–59
25210–GF–Plate2–103
25210–GF–Plate1–91
25210–WJL–Plate2–18
25183–WJL–Plate1–88
25183–GF–Plate1–4
25183–GF–Plate2–14
25210–WJL–Plate2–101
25183–GF–Plate2–22
25208–GF–Plate2–93
25208–GF–Plate1–72
25208–GF–Plate1–67
25208–GF–Plate2–86
25208–GF–Plate2–57
25208–GF–Plate1–19
25208–GF–Plate1–98
25208–GF–Plate1–26
25208–GF–Plate1–132
25208–GF–Plate2–35
25208–GF–Plate2–110
25208–GF–Plate2–7
Height
D.
-log10 (adjusted p-value)
log2 (Fold Change)
LysB
PGRP- SC1a
PGRP-SC1b
MtnA
CG30413
Cht4
CG11658
CG16965
CG13403
CG13135
CG1552
CG5162
CG8736
CG6271
CG12480
CG7203
E.
Normalized enrichment score
Enrichment p-value (rank)
actomyosin structure organization
cellular component assembly involved in morphogenesis
immune response
defense response
response to nutrient levels
response to extracellular stimulus
cellular response to extracellular stimulus
tRNA modification
F.
GF Inertia Gain
+Lp^WJL Inertia Gain
G.
SD decreased by Lp^WJL
SD increased by Lp^WJL
GF
+Lp^WJL
log2(count per million)
Ssrp
ckd
CG2263
pot
Vha36-3
I(1)G0156
CG43349
CG4764
CG9555
pyd3
CG1371
CG11594
CG3777
CG9836
CG42729
CG1319
CG11899
CG7916
CG32249
Lsp1gamma
Lcp2
Lsp1alpha
Lsp1beta
H.
+Lp^WJL SD
GF SD
Lsp1alpha
Lsp1beta
Lsp1gamma
CG42729
CG32249
CG7916
CG11594
CG11899
pyd3
CG3777
CG1319
CG9555
Vha36-3
ckd
CG4764
CG43349
CG9836
CG1371
Ssrp
I(1)G0156
CG2263
pot
I.
Strain ID
25183
25208
25210
Repressed
Not-induced
Induced
Transcripts
+Lp^WJL SD
GF SD

Figure S2

Figure S2. The single-larva BRB-seq indicates transcriptomic buffering in developmental genes by *Lp*^{WJL}. Related to Figure 1

A). Experimental setup to perform BRB-seq-based transcriptomics on individual larvae. Flies from three DGRP strains were reared in GF conditions. Egg-laying was synchronized and embryos were transferred to food caps: three left germ-free (1X PBS) and three inoculated with *Lp*^{WJL} (OD 0.5 in 1x PBS). At day 4, single larvae were collected from all plates, RNA extraction and RNA sequencing were performed. 12 larvae were collected per line for each condition, totaling 72 single larval transcriptomes.

B). Principal component plot of the corrected expression data after batch correction.

C). Hierarchical clustering of the transcriptomic data using the Ward's method. A batch effect of plate was corrected prior to clustering. The genotypes are color-coded (Green: 25210, violet: 25208, black: 25183). The red "branches" of the cluster represent GF samples, and green ones represent mono-associated samples.

D). The observed effect of *Lp*^{WJL} mono-association on gene expression is consistent with our previous findings, thus validating our transcriptome approach on individual larvae. The horizontal grey line represents the 0.05 FDR-corrected p-value threshold. The vertical lines are the -2 and 2 log2 (Fold Change) thresholds. Genes in red are significantly up-regulated, genes in blue are significantly down-regulated. Several representative genes of the top differentially regulated genes from each category are highlighted.

E). Gene set enrichment analysis on biological process gene ontology (GO) terms based on the effect of *Lp*^{WJL} mono-association. Gene sets in orange were derived from GLAD(Hu et al., 2015), whereas green gene sets were extracted from GO2MSIG(Powell, 2014).

F). Inertia gain of the HCPC analysis from Figure 1G and 1H. the black bars represent the "optimal" level of division of the tree suggested by FactoMineR.

G). Scatterplot of the standard deviation in expression level of each gene in the GF and *Lp*^{WJL} mono-associated condition. The black line represents the theoretical slope of 1 and intercept 0. The red line is a linear fit of the points. Labelled genes show the highest relative change in their standard deviation, as determined by the absolute value of $\log_2(SD_{LpWJL}/SD_{GF})$.

H). Box and whiskers plots showing the expression levels of genes with high relative change in standard deviation, regardless whether the genes themselves were up- or down-regulated.

I). Scatterplots of standard deviations of each gene calculated by genotype. Genes were faceted by how their differential expression alters within each strain in both GF and *Lp*^{WJL} mono-associated conditions: repressed (top panel), non-induced (middle panel) and induced (bottom panel). The black lines represent the theoretical slope of 1 and intercepts 0, the grey lines are the linear fit to the data. Since transcripts specifically modulated by *Lp*^{WJL} tend to have incomparable SD, we assessed GO enrichment only on non-differentially expressed genes (**see Fig.1K**)

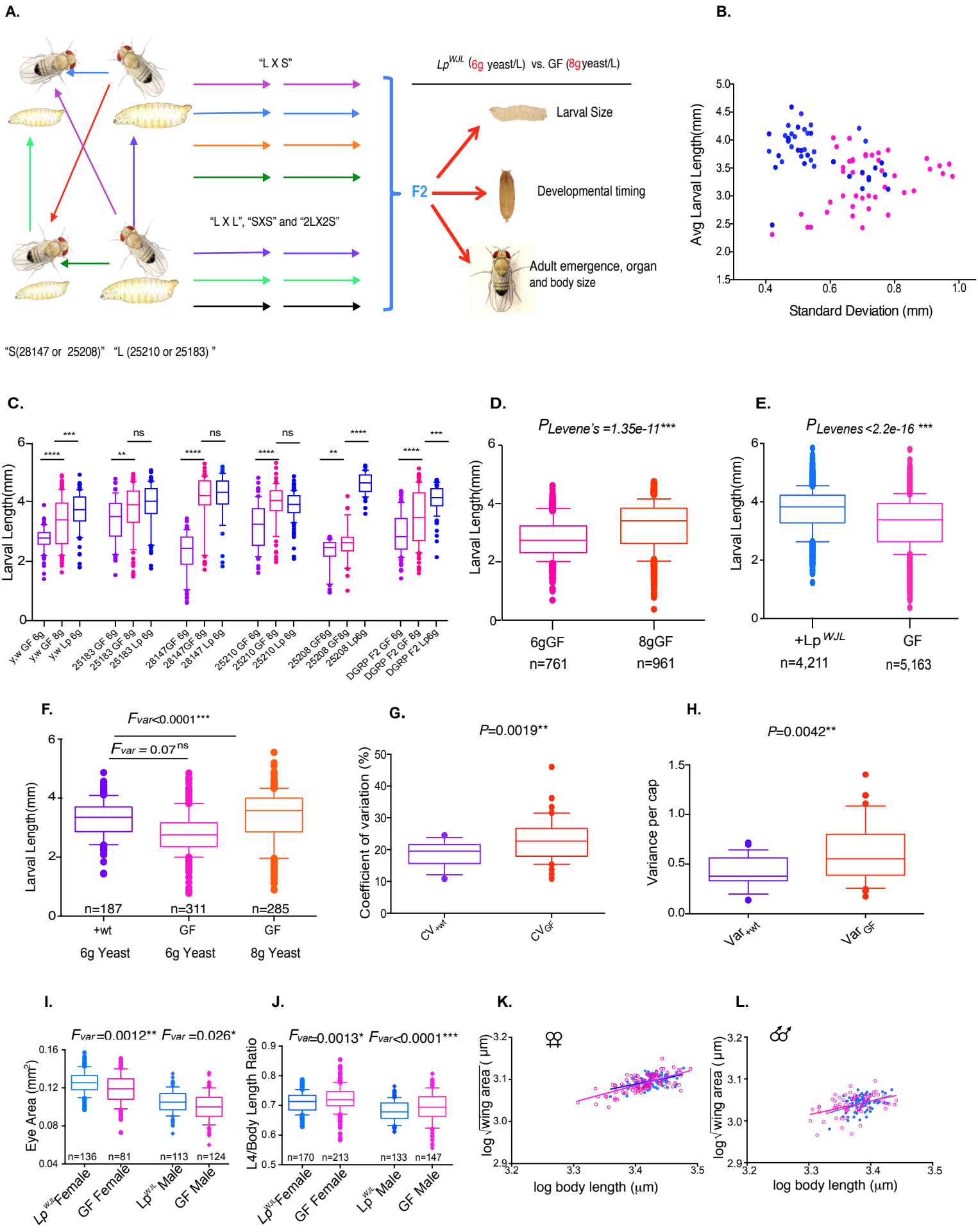
A.
"L X S"
"L X L", "SXS" and "2LX2S"
"S(28147 or 25208)" "L (25210 or 25183) "
Lp^WJL (6g yeast/L) vs. GF (8g yeast/L)
F2
Larval Size
Developmental timing
Adult emergence, organ and body size
B.
Avg Larval Length(mm)
Standard Deviation (mm)
C.
Larval Length(mm)
y,w GF 6g
y,w GF 8g
y,w Lp 6g
25183 GF 6g
25183 GF 8g
25183 Lp 6g
28147GF 6g
28147GF 8g
28147 Lp 6g
25210 GF 6g
25210 GF 8g
25210 Lp 6g
25208 GF6g
25208 GF8g
25208 Lp6g
DGRP F2 GF 6g
DGRP F2 GF 8g
DGRP F2 Lp6g
D.
P Levene's =1.35e-11***
Larval Length(mm)
6gGF
n=761
8gGF
n=961
E.
P Levenes <2.2e-16 ***
Larval Length(mm)
+Lp WJL
n=4,211
GF
n=5,163
F.
Fvar<0.0001***
Fvar = 0.07ns
Larval Length(mm)
n=187
n=311
n=285
+wt
GF
GF
6g Yeast
6g Yeast
8g Yeast
G.
P=0.0019**
Coefficient of variation (%)
CV+wt
CVGF
H.
P=0.0042**
Variance per cap
Var+wt
Var GF
I.
Fvar=0.0012** Fvar =0.026*
Eye Area (mm2)
n=136
n=81
n=113
n=124
Lp WJL Female
GF Female
Lp WJL Male
GF Male
J.
Fvar=0.0013* Fvar<0.0001***
L4/Body Length Ratio
n=170
n=213
n=133
n=147
Lp WJL Female
GF Female
Lp WJL Male
GF Male
K.
log √wing area (µm)
log body length (µm)
L.
log √wing area (µm)
log body length (µm)

Figure S3

Figure S3 In the genetically diverse DGRP F_2 population, *Lp*^{WJL} reduces variation in different physical fitness traits. Related to Figure 2

A). A diagram illustrating DGRP crosses to generate the F_2 generation for studying variation in larval size, pupariation and adult emergence. 25210 (RAL-859), 25183(RAL-335) are the lines with the "large" ("L") larvae as germ-free, and 25208(RAL-820) and 28147(RAL-158) are the lines with the "small" larvae as germ-free ("S"). Seven possible crosses are set up: 25210X25183 ("LXL"), 25208X28147("SXS"), 25210X25208, 25183X25208, 25210X28147, 25183X28147 are the four "LXS" crosses, and 25183 and 25210 X 25208 and 28147 is the "2L X 2S" cross.

B). A scatter plot showing how standard deviation (SD) changes as a function of larval length, and how such change differs in the DGRP F_2 GF (pink) and *Lp*^{WJL} mono-associated (blue) populations (see also Figure 2a and Methods for detailed schemes). Each data point represents the intercept of an SD value and its corresponding average larval length in a particular cross. Each SD and average length was derived from larvae measurements gathered from at least 3 biological replicates from either GF or *Lp*^{WJL} mono-associated conditions. Each replicate contains 10-40 larvae.

C). Larval lengths of axenic flies grown on media containing 6g (purple), 8g (pink) or 6g yeast with *Lp*^{WJL} inoculation (dark blue) on day 7 after egg-lay. Note that 2g extra yeast invariably boosts germ-free growth in different strains and genetic background. The asterisks indicate statistics differences when comparing average larval lengths between conditions.

D). Larval growth and variability comparison in DGRP F2 axenic larvae pooled from the parental strains (Figure S3C). For GF larvae raised on 6g/L yeast, average larval length =2.76mm, SD=0.66mm, CV=24.1%; for GF larvae raised on 8g/L yeast, average larval length =3.34mm, SD=0.85mm, CV=25.2%.

E). Box and Whisker graph illustrating the average length and standard deviation from pooled GF (pink) and *Lp*^{WJL} mono-associated DGRP (blue) F2 larvae, pooled from all the crosses in all three different repeats (Average GF larval length: 3.29mm; average Lp mono-associated larval length: 3.71mm; CV_{GF}=24.9%, CV_{Lp}=19.5%).

F). One representative experiment showing that re-associating the field-collected flies tends to buffer the variability in body length in size-matched larvae. The purple box represents body length from wild larvae grown on media contaminated with their untreated parents' fecal matter. Average GF larval length grown on 6g/L yeast media: 2.81mm; average GF larval length grown on 8g/L yeast media: 3.36mm: average re-associated larval length ("+wt"): 3.07 mm; P= 0.338. CV_{GF} (6g/L, pink) = 24.9%, CV_{GF} (8g/L, orange)= 27.0%, CVwt (purple)= 18.9%.

G). and H). The compiled CV values (**e**.) and variances (**f**.) derived from each low-yeast cap containing 40~50 field-collected larvae. The average CV and variance are lower in the population re-associated with its own microbes (purple) than in the GF population (orange)

I). In both male (lozenge) and female (circle) adults, the variances in eye size are greater in GF F_2 progeny. The difference in mean eye area, for females P<0.0001***; for males, P=0.0013**.

J). The length of the L4 vein in the wing is used as a proxy of the wing length. In the accumulated ratios of wing length over body length, the variances are greater in the GF flies (The difference in average L4/ body length, for females P<0.0028**; for males, P=0.02*).

K). and L). Scatter plots illustrating the allometric relationship between wing area and body size in female (i) and male (j) DGRP F_2 adults. Pink open circles: GF, blue filled circles: *Lp*^{WJL}. Each line represents the allometric slope of the data points shown by the same color. Either in males or females, there is no difference in allometric slope between the GF and mono-associated population. For GF females, Y_{GF} = 0.3963*X + 1.738, 95%C.I.= 0.3117 to 0.4810; for *Lp*^{WJL} females, Y_{Lp} = 0.2978*X + 2.076, 95%C.I.= 0,1785 to 0,4172, P=0.203, n.s ; for GF males, Y_{GF} = 0.3261*X + 1.939, 95%C.I.= 0.1725 to 0.4796 ; for *Lp*^{WJL} males, Y_{Lp}= 0.4141*X + 1.639, 95% C.I. =0.1842 to 0.6439, P=0.55, ns. Data are represented as Mean and 10-90 percentile in all panels.

A.

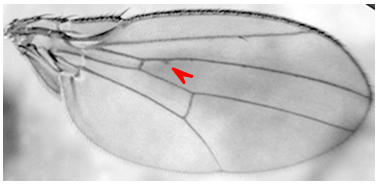

B.

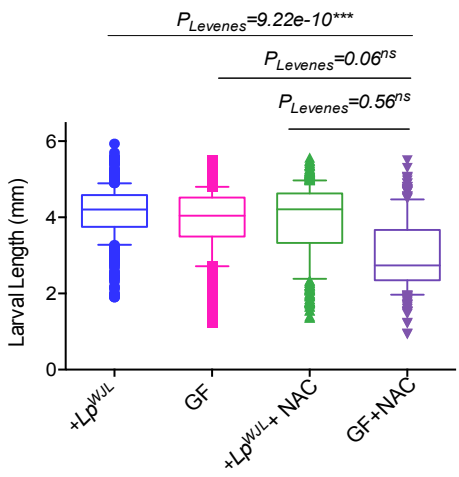

C.

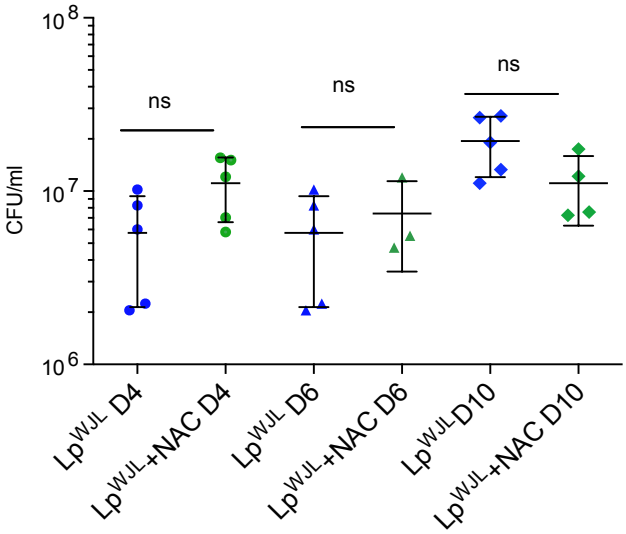

Figure S4

Figure S4 The LpWJL buffering in developmental trait and organ patterning robustness involves ROS signaling. Related to Figure 3 and 4.

A.) An image of a wing of an Lp^{WJL} adult is shown, as a representation of the most visible "defect" ever observed in mono-associated adults. Red arrow points to the subtle vein tissue thickening. We included these as "defects" in the Lp^{WJL} F_2 population in the analyses presented in Figure 3A, 3B, and 4F.

B). Germ-free larvae (light violet) that ingested NAC show comparable size variation to Lp^{WJL} larvae fed on NAC (McFall-Ngai et al.) or germ-free larvae who have not been exposed to NAC (pink).

C). Bacterial niche load (NL) evolution ("Niche" is defined as the substrate with both larvae and bacteria present) during the course of larval development with Lp^{WJL} with or without NAC treatment (Day 4, Day 6 and Day 10). Data are represented as mean ± SD.

TableS1. Average D7 larvae length for individual DGRP lines. Related to Figure 1

DGRP Lines	GF* Length(mm)	GF SD*(mm)	*Lp*^{WJL} * Length(mm)	*Lp*^{WJL} SD(mm)	*Lp*^{WJL}/GF Ratio
25174	2.193	0.584	3.637	0.895	1.658
25175	2.693	0.687	4.496	0.659	1.670
25176	1.443	0.536	3.903	0.648	2.704
25180	2.151	0.454	3.795	0.635	1.764
25181	2.374	0.824	4.224	0.946	1.779
25182	2.108	0.451	3.293	0.859	1.562
25183	2.961	0.657	4.066	0.548	1.373
25184	1.957	0.53	4.323	0.587	2.209
25185	2.459	0.681	3.93	0.722	1.598
25186	2.278	0.667	4.289	0.803	1.883
25187	2.109	0.479	3.798	0.744	1.801
25188	2.253	0.421	4.202	0.786	1.865
25189	2.586	0.393	3.448	0.876	1.333
25190	2.292	0.512	3.976	0.941	1.735
25191	2.348	0.428	3.953	0.797	1.684
25192	2.194	0.401	4.145	0.731	1.889
25193	2.414	0.582	4.05	0.782	1.678
25194	2.506	0.558	4.195	0.508	1.674
25195	2.07	0.402	3.635	0.867	1.756
25197	1.944	0.397	3.73	0.734	1.919
25198	2.051	0.394	3.936	0.673	1.919
25199	1.514	0.524	3.78	0.753	2.497
25200	2.869	0.752	4.227	0.605	1.473
25201	2.182	0.347	4.186	0.601	1.918
25202	2.273	0.639	3.85	0.792	1.694
25203	1.541	0.513	4.158	0.755	2.698
25204	1.686	0.678	4.088	0.774	2.425
25205	2.351	0.567	3.77	0.606	1.604
25206	2.5	0.643	4.173	0.619	1.669
25207	2.028	0.481	3.896	0.811	1.921
25208	1.649	0.443	4.103	0.947	2.488
25209	2.187	0.67	4.232	0.819	1.935
25210	2.772	0.633	4.03	0.466	1.454
25445	2.01	0.468	3.956	0.668	1.968
25744	2.097	0.34	4.235	0.666	2.020
25745	2.501	0.612	4.051	0.599	1.620
28132	2.828	0.684	4.485	0.534	1.586
28134	1.854	0.383	4.144	0.479	2.235
28136	1.707	0.415	4.204	0.548	2.463
28138	1.38	0.487	4.318	0.693	3.129
28142	2.938	0.836	4.487	0.489	1.527
28146	2.077	0.36	4.564	0.915	2.197
28147	1.575	0.552	4.061	0.728	2.578
28153	2.298	0.329	3.97	0.541	1.728
28154	2.256	0.339	4.365	0.482	1.935
28160	2.51	0.662	4.118	0.714	1.640
28164	2.394	0.448	4.207	0.584	1.757
28166	2.163	0.402	4.489	0.642	2.075
28173	2.039	0.309	4.122	0.697	2.022
28192	2.141	0.506	4.286	0.659	2.002
28194	2.269	0.565	4.424	0.72	1.950
28197	2.89	0.742	4.547	0.519	1.573
28208	2.339	0.438	4.14	0.705	1.767

*GF: germ-free

**Lp*^{WJL}: Lactobacillus plantarum, stain name: WJL

*SD: standard deviation

Table S2 . Variants associated with the growth benefits conferred by *Lactobacillus plantarum* (*Lp*^{WJL}). Related to Figure 1.

Variants	R^2	P-value	Minor allele	Major allele	Ref* allele	MAF*	Variant Class	Molecular and cellular functions
CG13492	46.46%	1.23E-06	C	T	C	0.245	intron	Unknown
	45.81%	4.526E-07	T	A	T	0.244		
	45.56%	1.65E-06	G	A	G	0.25		
CG32683	39.04%	2.76E-06	A	T	T	0.2453	Intron/ downstream	Unknown, arrestin-like
	39.04%	2.76E-06	A	C	C	0.2453		
	29.32%	4.03E-06	T	A	A	0.22		
	29.07%	3.19E-06	T	G	G	0.2245		
	29.80%	1.17E-05	CTGTTG	C	C	0.283		
CG33269	35.58%	8.21e-06	G	A	A	0.14	Intergenic	Unknown
dpr6	33.06%	2.94E-05	A	T	T	0.1224	Intron	Immunoglobulin-like domain; sensory perception of chemical stimulus
	21.34%	7.77E-06	A	G	G	0.08		
Eip75B	32.65%	1.22E-05	C	T	C	0.1176	Intron	Nuclear hormone receptor, ecdysone response, antimicrobial humoral response
rg	32.14%	9.25E-06	G	A	G	0.4	Intron	PKA-binding, cone cell differentiation, mushroom body development, olfactory learning
sfl	27.37%	9.18E-06	G	T	T	0.4706	Intron	heparan sulfate proteoglycans (HSPGs) biosynthesis/wg morphogen diffusion
CG42669	26.66%	1.23E-05	A	G	G	0.1373	Intron	Supervillin, actin-binding
bol	25.07%	3.76E-06	C	T	T	0.2	3'UTR	RNA binding protein. Role in meiotic entry and germline differentiation
CR43427, lncRNA566	23.7%	4,53E-06	G	T	T	0.3269	intergenic	Unknown, lncRNA
daw	15.1%	4.45E-06	T	C	C	0.1837	Synonymous substitution	TGF-β ligand: growth; regulation of insulin secretion
arr	14.68%	1.69E-06	G	C	C	0.1875	intron	wnt protein binding/canonical wnt pathway
glut1	11.14%	1.56E-06	G	T	T	0.2245	intron	General glucose/sugar transporter

*MAF: minor allele frequency in the 53 DGRP lines
*Ref allele: allele info derived from BDGP (Berkeley Drosophila Genome Project)
R^2 reflects effect size

Table S3. Individual larval transcriptome sample list. Related to Figure 1

SampleID	Genotype	Treatment	Plate	Individual	Well_Row	Well_Column	TotalReads	Timepoint
GF-d4-Plate1-25183-4	25183	GF	Plate1	4	D	1	3374679	d4
WJL-d4-Plate1-25183-5	25183	WJL	Plate1	5	E	2	4323699	d4
GF-d4-Plate2-25208-7	25208	GF	Plate2	7	E	9	1537636	d4
GF-d4-Plate1-25210-10	25210	GF	Plate1	10	D	5	3969828	d4
WJL-d4-Plate1-25210-11	25210	WJL	Plate1	11	E	6	5131500	d4
GF-d4-Plate2-25183-14	25183	GF	Plate2	14	E	1	3307084	d4
WJL-d4-Plate2-25183-15	25183	WJL	Plate2	15	D	2	2816461	d4
GF-d4-Plate2-25210-17	25210	GF	Plate2	17	E	5	5063082	d4
WJL-d4-Plate2-25210-18	25210	WJL	Plate2	18	D	6	4162852	d4
GF-d4-Plate1-25208-19	25208	GF	Plate1	19	D	9	2459570	d4
WJL-d4-Plate2-25183-21	25183	WJL	Plate2	21	E	2	2399808	d4
GF-d4-Plate2-25183-22	25183	GF	Plate2	22	D	1	4448517	d4
WJL-d4-Plate2-25210-23	25210	WJL	Plate2	23	E	6	4508569	d4
GF-d4-Plate1-25208-26	25208	GF	Plate1	26	E	9	2085683	d4
WJL-d4-Plate1-25183-29	25183	WJL	Plate1	29	D	2	1843092	d4
GF-d4-Plate1-25183-30	25183	GF	Plate1	30	E	1	3678838	d4
GF-d4-Plate2-25208-35	25208	GF	Plate2	35	D	9	3470625	d4
WJL-d4-Plate1-25210-38	25210	WJL	Plate1	38	D	6	3828526	d4
GF-d4-Plate1-25210-39	25210	GF	Plate1	39	E	5	4247231	d4
GF-d4-Plate2-25183-41	25183	GF	Plate2	41	F	1	1761823	d4
GF-d4-Plate2-25210-43	25210	GF	Plate2	43	F	5	3169382	d4
WJL-d4-Plate1-25208-46	25208	WJL	Plate1	46	C	10	2892171	d4
WJL-d4-Plate1-25208-47	25208	WJL	Plate1	47	B	10	3387926	d4
WJL-d4-Plate1-25183-48	25183	WJL	Plate1	48	F	2	3595814	d4
WJL-d4-Plate1-25208-50	25208	WJL	Plate1	50	A	10	5708076	d4
WJL-d4-Plate1-25208-52	25208	WJL	Plate1	52	E	10	3305828	d4
WJL-d4-Plate1-25208-54	25208	WJL	Plate1	54	D	10	2980174	d4
WJL-d4-Plate1-25208-55	25208	WJL	Plate1	55	F	10	2648893	d4
GF-d4-Plate2-25208-57	25208	GF	Plate2	57	F	9	1789505	d4
GF-d4-Plate1-25183-59	25183	GF	Plate1	59	F	1	3461758	d4
GF-d4-Plate1-25210-60	25210	GF	Plate1	60	F	5	3205718	d4
WJL-d4-Plate2-25183-64	25183	WJL	Plate2	64	F	2	3165014	d4
GF-d4-Plate1-25208-67	25208	GF	Plate1	67	F	9	1551867	d4
WJL-d4-Plate2-25210-70	25210	WJL	Plate2	70	F	6	8073425	d4
GF-d4-Plate1-25208-72	25208	GF	Plate1	72	C	9	2668655	d4
GF-d4-Plate2-25210-74	25210	GF	Plate2	74	B	5	947737	d4
WJL-d4-Plate2-25210-75	25210	WJL	Plate2	75	C	6	4812520	d4
GF-d4-Plate2-25183-78	25183	GF	Plate2	78	B	1	2869820	d4
WJL-d4-Plate2-25183-79	25183	WJL	Plate2	79	C	2	4934533	d4
GF-d4-Plate1-25210-83	25210	GF	Plate1	83	C	5	4113175	d4
WJL-d4-Plate1-25210-84	25210	WJL	Plate1	84	B	6	4684552	d4
GF-d4-Plate2-25208-86	25208	GF	Plate2	86	B	9	3324070	d4
GF-d4-Plate1-25183-87	25183	GF	Plate1	87	C	1	3728767	d4
WJL-d4-Plate1-25183-88	25183	WJL	Plate1	88	B	2	4564509	d4
WJL-d4-Plate1-25210-90	25210	WJL	Plate1	90	C	6	3714293	d4
GF-d4-Plate1-25210-91	25210	GF	Plate1	91	B	5	4179985	d4
GF-d4-Plate2-25208-93	25208	GF	Plate2	93	C	9	3569201	d4
WJL-d4-Plate1-25183-94	25183	WJL	Plate1	94	C	2	4200621	d4
GF-d4-Plate1-25183-95	25183	GF	Plate1	95	B	1	4373035	d4
GF-d4-Plate1-25208-98	25208	GF	Plate1	98	B	9	3652231	d4
WJL-d4-Plate2-25210-101	25210	WJL	Plate2	101	B	6	4457721	d4
GF-d4-Plate2-25210-103	25210	GF	Plate2	103	C	5	3903565	d4
WJL-d4-Plate2-25183-104	25183	WJL	Plate2	104	B	2	982388	d4
GF-d4-Plate2-25183-105	25183	GF	Plate2	105	C	1	3094592	d4
GF-d4-Plate2-25208-110	25208	GF	Plate2	110	A	9	1967561	d4
WJL-d4-Plate1-25210-112	25210	WJL	Plate1	112	A	6	3472086	d4
WJL-d4-Plate1-25183-116	25183	WJL	Plate1	116	A	2	4865847	d4
GF-d4-Plate2-25210-119	25210	GF	Plate2	119	A	5	3773438	d4
WJL-d4-Plate2-25208-120	25208	WJL	Plate2	120	F	10	2018688	d4
WJL-d4-Plate2-25208-121	25208	WJL	Plate2	121	D	10	2595705	d4
WJL-d4-Plate2-25208-123	25208	WJL	Plate2	123	E	10	1841390	d4
WJL-d4-Plate2-25208-124	25208	WJL	Plate2	124	A	10	3326544	d4
GF-d4-Plate2-25183-125	25183	GF	Plate2	125	A	1	1822797	d4
WJL-d4-Plate2-25208-126	25208	WJL	Plate2	126	B	10	3831425	d4
WJL-d4-Plate2-25208-127	25208	WJL	Plate2	127	C	10	3109485	d4
WJL-d4-Plate2-25210-129	25210	WJL	Plate2	129	A	6	1737064	d4
GF-d4-Plate1-25208-132	25208	GF	Plate1	132	A	9	3284211	d4
WJL-d4-Plate2-25183-135	25183	WJL	Plate2	135	A	2	4603643	d4
GF-d4-Plate1-25210-139	25210	GF	Plate1	139	A	5	2749602	d4
GF-d4-Plate1-25183-140	25183	GF	Plate1	140	A	1	2722703	d4

Transparent Methods

•Fly stocks and genetic crosses

Drosophila were kept at 25°C in a Panasonic Mir425 incubator with 12/12 hrs dark/light cycles. Routine stocks were kept on standard laboratory diet (see below "media preparation and NAC treatment") The 53 DGRP lines were obtained from Bloomington Drosophila Stock Center.

Field-collected flies were trapped with rotten tomatoes in a garden in Solaize (France) and reared on a medium without chemical preservatives to minimize the modification to their gut microbiota(Tefit et al., 2017). One liter of media contains 15g inactivated yeast, 25g sucrose (Sigma Aldrich, ref. #84100), 80g cornmeal and 10g agar.

To generate DGRP F_2s, four DGRP lines were selected for setting up seven different crosses: 25210 (RAL-859), 25183(RAL-335) are the lines with "large" larvae as germ-free, and 25208(RAL-820) and 28147(RAL-158) are the line with "small" larvae as germ-free (see figure legend Figure S3a).

All RNAi lines were crossed to the driver line *y,w;; tubulin*-GAL80^{ts} ,*daugtherless*-GAL4. To minimize lethality, we dampend the GAL4 strength by leaving the genetic crosses at 25°C. The following fly strains were used: *y,w*, UAS-*dpr-6*-IR(P{KK112634}VIE-260B), UAS-*CG13492*-IR, (w^{1118};P{GD14825}v29390), UAS-*daw*-IR(NIG #16987R-1), UAS-*sfl*-IR (w^{1118}; P{GD2336}v5070), UAS-*arr*-IR (w^{1118}; P{GD2617}v4818), UAS-*rg*-IR(w^{1118}; P{GD8235}v17407), UAS-*bol*-IR(w^{1118}; {GD10525}v21536), UAS-*glut1*-IR(y^1 v^1; P{TRiP.JF03060}attP2, Bloomington 28645), UAS-*CG32683*-IR (P{KK112515}VIE-260B), UAS-*CG42669*-IR(w^{1118};P{GD7292}v18081), UAS-*Eip75B*-IR (w^{1118}; P{GD1434}v44851), UAS-*mCherry*-IR (y^1 v^1; P{CaryP}attP2), VDRC GD control (VDRC ID60000).

•GWAS and data computing of heritability indice

To calculate heritability, we estimated variance components using a random effects model using the lme4 R package(Bates, 2015). To infer the differences in heritability between GF and Lp^{WJL}-monoassociated conditions, we chose to use a bootstrap approach as in (https://github.com/famuvie/breedR/wiki/Heritability). Strains and experiment dates were treated as random effects, and the heritability was calculated as VA/(VA+VD+VR), where VA is the additive genetic variance, and is equal to twice the Strain variance, VD is the experiment date variance, and VR is the residual variance. For the estimation of the empirical distribution of heritability indices, a bootstrap method within the R breedR package was used for 1000 simulations per condition. We used the online tool specifically designed for the DGRPs (http://dgrp2.gnets.ncsu.edu/)(Huang et al., 2014; Mackay et al., 2012) for GWAS. The Manhattan and QQ-plots were generated using R. Raw GWAS data can be accessed at https://data.mendeley.com/datasets/5m9ghb7vbs/4

•Single larva transcriptome analysis

RNA extraction from single larvae: Larvae were handpicked under the microscope using forceps and transferred to Eppendorf tubes filled with 100uL of beads and 350 uL of Trizol. The samples were then homogenized using a Precellys 24 Tissue Homogenizer at 6000 rpm for 30 seconds. After homogenization, the samples were transferred to liquid nitrogen for flash freezing and stored at –80°C. For RNA extraction, samples were thawed on ice, 350 uL of 100% Ethanol was then added to each sample before homogenizing again with the same parameters. Direct-zol™ RNA Miniprep R2056 Kit was used to extract RNA with these modifications: DNAse I treatment was skipped; after the RNA Wash step, an extra 2 min centrifugation step was added to remove residual wash buffer. Lastly, the sample was eluted in 10 uL of water, incubated at room

temperature for 2 min and then spun for 2 min to collect RNA. RNA was transferred to a low-binding 96 well plate and stored at -70°C.

RNA-sequencing: We prepared the libraries using the BRB-seq protocol and sequenced them using an Illumina NextSeq 500 (Alpern et al., 2018). Reads from the BRB-seq protocol generates two fastq files: R1 containing barcodes and UMIs and R2 containing the read sequences. R2 fastq file was first trimmed for removing BRB-seq-specific adapter and polyA sequences using the BRB-seqTools v1.0 suite (available at http://github.com/DeplanckeLab/BRB-seqTools). We then aligned the trimmed reads to the Ensembl r78 gene annotation of the dm3 genome mixed with *the Lactobacillus Plantarum WJL* genome using STAR (Version 2.5.3a)(Dobin et al., 2013), with default parameters (and extra "--outFilterMultimapNmax 1" parameter for completely removing multiple mapped reads). Then, using the BRB-seqTools v1.0 suite (available at http://github.com/DeplanckeLab/BRB-seqTools), we performed simultaneously the sample demultiplexing, and the count of reads per gene from the R1 FASTQ and the aligned R2 BAM files. This generated the count matrix that was used for further analyses. Genes were retained in the analysis if they had more than 10 reads in more than 50 samples. The data was subsequently transformed using the voom method. Differential expression was performed using the R Limma package(Law et al., 2014; Ritchie et al., 2015). Genes with a $\log_2$ fold change greater than 2 and a Benjamini-Hochberg adjusted P-value less than 0.05 were considered differentially expressed. Since the library preparation was performed in two plates, hence introducing a batch effect, we used the duplicateCorrelation function and included the batch as a blocking variable. Prior to PCA analysis and standard deviation calculations, we removed the batch effect using the removeBatchEffects function and then used the princomp function. We used the cluster profiler package to perform GSEA analyses. The gmt file containing the gene ontology annotations was obtained from GO2MSIG data. Specifically, we used the highquality GO annotations for *Drosophila melanogaster*. For each GSEA analysis, we used 100,000 permutations to obtain adjusted p-values and only included gene set sizes to between 6 and 1000 genes. The raw expression data has been deposited in ArrayExpress (accession number: E-MTAB-6518)

RNA-sequencing: We prepared the libraries using the BRB-seq protocol and sequenced them using an Illumina NextSeq 500(Alpern et al., 2018). Reads from the BRB-seq protocol generates two fastq files: R1 containing barcodes and UMIs and R2 containing the read sequences. R2 fastq file was first trimmed for removing BRB-seq-specific adapter and polyA sequences using the BRB-seqTools v1.0 suite (available at http://github.com/DeplanckeLab/BRB-seqTools). We then aligned the trimmed reads to the Ensembl r78 gene annotation of the dm3 genome mixed with *the Lactobacillus Plantarum WJL* genome using STAR (Version 2.5.3a)(Dobin et al., 2013), with default parameters (and extra "--outFilterMultimapNmax 1" parameter for completely removing multiple mapped reads). Then, using the BRB-seqTools v1.0 suite (available at http://github.com/DeplanckeLab/BRB-seqTools), we performed simultaneously the sample demultiplexing, and the count of reads per gene from the R1 FASTQ and the aligned R2 BAM files. This generated the count matrix that was used for further analyses. The data was subsequently transformed using the voom method and analyzed using the R Limma package(Law et al., 2014; Ritchie et al., 2015).

The raw expression data of BRB-Seq has been deposited in ArrayExpress (accession number: E-MTAB-6518)

•The making and maintenance of germ-free flies

Axenic flies were generated by dechorionating embryos with 50% household bleach for five minutes; eggs were then washed in successive 70% ethanol and sterile distilled water for three minutes each. After washing, eggs were transferred to tubes containing standard diet and a

cocktail of antibiotics containing 50µg/mL ampicillin, 50µg/mL kanamycin, 15µg/mL erythromycin, 50µg/mL tetracyclin for stock maintenance. Axeny was routinely verified by plating larvae and adult lysates on LB and MRS plates. For experiments food without antibiotics was used.

•Media preparation and NAC treatment

Standard laboratory fly food consists of 50g/L inactivated yeast (Springaline™), 80g/L cornmeal, 7.14g/L agar, 5.12g/L Moldex (Sigma M-50109) and 0.4% propionic acid. Where applicable, experiments comparing variations in larval size, developmental timing, adult emergence were performed on diet with 6g or 8g inactivated yeast per liter of media while keeping the same concentrations for the other ingredients. Where appropriate, 1.7g/L of N-Acetylcystein (SigmaA7250-25g) was added to the low-protein diet.

•Larval Length Measurement

All live *Drosophila* larvae were collected from each nutritive cap containing low yeast diet by temporary immersion in sterile PBS, transferred on a microscopy slide, killed with a short pulse of heat (5 sec at 90°C), mounted with 80% glycerol/PBS. The images were taken with the Leica stereomicroscope M205FA and the lengths of individual larvae were measured using ImageJ software(Schneider et al., 2012). For each DGRP strain and each cross and/or condition, at least three biological replicates were generated.

•Developmental timing and Adult emergence

Developmental timing and adult emergence of the flies were quantified by counting the number of individuals appearing every 24 hours until the last pupa/adult emerges. Each animal is assigned to the number that corresponds to the day it appeared, and the population mean and variance were calculated based on the cumulative numbers.

•Adult trait measurements

2-3 days old adult flies were anesthetized with CO_2 and immersed in 70% ethanol, and individual body and its corresponding organ (wing and eye) were imaged under a Leica M205 stereomicroscope. Specifically, the adult body length was measured from the top of the head to the tip of the abdomen. The eye area was measured by manually tracing the circumference of both eyes. The wings were gently nipped at the base of the hinge and imaged, and the area was measured by tracing the edge of the wing. All images were taken measured using ImageJ software

•Bacteria culture and mono-association

For each mono-association experiment, Lp^{WJL} (Ryu et al., 2008) was grown in Man, Rogosa and Sharpe (MRS) medium (Difco, ref. #288110) over-night at 37°C, and diluted to O.D.=0.5 the next morning to inoculate 40 freshly laid eggs on a 55mm petri dish or standard 28mm tubes containing fly food of low yeast content. The inoculum corresponds to about $5x10^7$ CFUs. Equal volume of sterile PBS was spread on control axenic eggs.

To contaminate the garden-collected flies with their own microbiota, eggs were dechorionated and directly seeded onto appropriate food caps. Sterile PBS was used to wash the side of the bottles where the adult wild flies were raised to recover more fecal content, and 300 ul of the wash was inoculated to the dechorionated eggs. For GF control, 300 ul of sterile PBS was used to inoculate the dechorionated eggs. The microbial composition of this community can be founded here(Tefit et al., 2017).

•Bacteria niche load

Five to six 24 hour old germ-free larvae were collected from the low-protein diet food cap and transferred to a microtube containing 400ul of low-protein diet, and inoculated with 50ul of Lp^{WJL} of 0.5 O.D.. On the day of harvest, ~0.75-1mm glass micro-beads and 900µl PBS were added to each microtube and the entire content of the tube was homogenized with the Precellys-24 tissue homogenizer (Bertin Technologies). Lysate dilutions (in PBS) are plated on MRS agar with Easyspiral automatic plater (Intersciences). The MRS agar plates were incubated for 24h at 37°C. The CFU/ml count was calculated based on the readings by the automatic colony counter Scan1200 (Intersciences)

•Statistical Analysis and data representation

GraphPad Prism software version 6.0f for Macintosh (GraphPad Software, La Jolla California USA, www.graphpad.com) was used to compare GF and Lp^{WJL}-associated conditions for larval length, developmental timing, adult emergence, allometry and linear regression analysis for the buffering effect. For small samples with less than 10 data points, nonparametric analysis was conducted. For all each sample set, we first conducted D'agostino-Pearson normality test. If the samples assume normal distribution, the F test of equality of variances were conducted to compare variability among the datasets. For samples assuming non-normal distribution, Levene's test is conducted based on the deviation from the median of each dataset.

Supplemental Reference

Alpern, D., Gardeux, V., Russeil, J., and Deplancke, B. (2018). Time- and cost-efficient high-throughput transcriptomics enabled by Bulk RNA Barcoding and sequencing. bioRxiv.

Bates, D., Mâchler M, Bolker B, Walker S (2015). Fitting Linear Mixed-Effects Models Using lme4. Journal of Statistical Software *67*, 1-48.

Dobin, A., Davis, C.A., Schlesinger, F., Drenkow, J., Zaleski, C., Jha, S., Batut, P., Chaisson, M., and Gingeras, T.R. (2013). STAR: ultrafast universal RNA-seq aligner. Bioinformatics *29*, 15-21.

Hu, Y., Comjean, A., Perkins, L.A., Perrimon, N., and Mohr, S.E. (2015). GLAD: an Online Database of Gene List Annotation for Drosophila. J Genomics *3*, 75-81.

Huang, W., Massouras, A., Inoue, Y., Peiffer, J., Ramia, M., Tarone, A.M., Turlapati, L., Zichner, T., Zhu, D., Lyman, R.F., *et al.* (2014). Natural variation in genome architecture among 205 Drosophila melanogaster Genetic Reference Panel lines. Genome Res *24*, 1193-1208.

Law, C.W., Chen, Y., Shi, W., and Smyth, G.K. (2014). voom: Precision weights unlock linear model analysis tools for RNA-seq read counts. Genome Biol *15*, R29.

Mackay, T.F., Richards, S., Stone, E.A., Barbadilla, A., Ayroles, J.F., Zhu, D., Casillas, S., Han, Y., Magwire, M.M., Cridland, J.M., *et al.* (2012). The Drosophila melanogaster Genetic Reference Panel. Nature *482*, 173-178.

McFall-Ngai, M., Hadfield, M.G., Bosch, T.C., Carey, H.V., Domazet-Loso, T., Douglas, A.E., Dubilier, N., Eberl, G., Fukami, T., Gilbert, S.F., *et al.* (2013). Animals in a bacterial world, a new imperative for the life sciences. Proc Natl Acad Sci U S A *110*, 3229-3236.

Powell, J.A. (2014). GO2MSIG, an automated GO based multi-species gene set generator for gene set enrichment analysis. BMC Bioinformatics *15*, 146.

Ritchie, M.E., Phipson, B., Wu, D., Hu, Y., Law, C.W., Shi, W., and Smyth, G.K. (2015). limma powers differential expression analyses for RNA-sequencing and microarray studies. Nucleic Acids Res *43*, e47.

Ryu, J.H., Kim, S.H., Lee, H.Y., Bai, J.Y., Nam, Y.D., Bae, J.W., Lee, D.G., Shin, S.C., Ha, E.M., and Lee, W.J. (2008). Innate immune homeostasis by the homeobox gene caudal and commensal-gut mutualism in Drosophila. Science *319*, 777-782.

Schneider, C.A., Rasband, W.S., and Eliceiri, K.W. (2012). NIH Image to ImageJ: 25 years of image analysis. Nat Methods *9*, 671-675.

Tefit, M.A., Gillet, B., Joncour, P., Hughes, S., and Leulier, F. (2017). Stable association of a Drosophila-derived microbiota with its animal partner and the nutritional environment throughout a fly population's life cycle. J Insect Physiol.